



HAL
open science

MATRIX (Multiconfiguration Aerosol TRacker of mIXing state): an aerosol microphysical module for global atmospheric models

S. E. Bauer, D. Wright, D. Koch, E. R. Lewis, R. Mcgraw, L.-S. Chang, S. E. Schwartz, R. Ruedy

► **To cite this version:**

S. E. Bauer, D. Wright, D. Koch, E. R. Lewis, R. Mcgraw, et al.. MATRIX (Multiconfiguration Aerosol TRacker of mIXing state): an aerosol microphysical module for global atmospheric models. Atmospheric Chemistry and Physics Discussions, 2008, 8 (3), pp.9931-10003. hal-00304204

HAL Id: hal-00304204

<https://hal.science/hal-00304204>

Submitted on 18 Jun 2008

HAL is a multi-disciplinary open access archive for the deposit and dissemination of scientific research documents, whether they are published or not. The documents may come from teaching and research institutions in France or abroad, or from public or private research centers.

L'archive ouverte pluridisciplinaire **HAL**, est destinée au dépôt et à la diffusion de documents scientifiques de niveau recherche, publiés ou non, émanant des établissements d'enseignement et de recherche français ou étrangers, des laboratoires publics ou privés.

MATRIX (Multiconfiguration Aerosol TRacker of mIXing state): an aerosol microphysical module for global atmospheric models

S. E. Bauer¹, D. Wright³, D. Koch¹, E. R. Lewis², R. McGraw², L.-S. Chang⁴,
S. E. Schwartz², and R. Ruedy⁵

¹The Earth Institute at Columbia University and NASA Goddard Institute for Space Studies,
New York, USA

²Brookhaven National Laboratory, Upton, New York, USA

³School of Arts and Sciences, Rutgers University, New Brunswick, NJ 08901, USA

⁴Global Research Center, National Institute of Environmental Research, Kyungseo-dong
Seo-gu, Incheon, Korea

⁵Sigma Space Partners (SSP) and NASA Goddard Institute for Space Studies, New York, USA

Received: 26 March 2008 – Accepted: 15 April 2008 – Published: 29 May 2008

Correspondence to: S. E. Bauer (sbauer@giss.nasa.gov)

Published by Copernicus Publications on behalf of the European Geosciences Union.

Title Page

Abstract

Introduction

Conclusions

References

Tables

Figures

◀

▶

◀

▶

Back

Close

Full Screen / Esc

Printer-friendly Version

Interactive Discussion



Abstract

A new aerosol microphysical module MATRIX, the Multiconfiguration Aerosol TRacker of mIXing state, and its application in the Goddard Institute for Space Studies (GISS) climate model (ModelE) is described. This module, which is based on the quadrature method of moments (QMOM), represents nucleation, condensation, coagulation, internal and external mixing, and cloud-drop activation and provides aerosol particle mass and number concentration and particle size information for up to 16 mixed-mode aerosol populations. Internal and external mixing among aerosol components sulfate, nitrate, ammonium, carbonaceous aerosols, dust and sea-salt particles are represented. The solubility of each aerosol mode, which is explicitly calculated based on its soluble and insoluble components, enables calculation of the dependence of cloud drop activation on the microphysical characterization of multiple soluble modes. A detailed model description and results of box-model simulations of various mode configurations are presented. The number concentration of aerosol particles activated to cloud drops depends on the mode configuration. Simulations on the global scale with the GISS climate model are evaluated against aircraft and station measurements of aerosol mass and number concentration and particle size. The model accurately captures the observed size distributions in the aiten and accumulation modes up to particle diameter 1 μm , in which sulfate, nitrate, black and organic carbon are predominantly located; however the model underestimates coarse-mode number concentration and size, especially in the marine environment.

1 Introduction

The impact of natural and anthropogenic aerosols on the climate system is the subject of numerous laboratory, experimental and theoretical studies (Ghan and Schwartz, 2007). These studies span spatial and temporal scales of several orders of magnitudes. Global climate models at the upper end of those time scales are the ultimate

ACPD

8, 9931–10003, 2008

MATRIX

S. E. Bauer et al.

Title Page

Abstract

Introduction

Conclusions

References

Tables

Figures

◀

▶

◀

▶

Back

Close

Full Screen / Esc

Printer-friendly Version

Interactive Discussion



5 tool to estimate the integrative impacts of aerosols on climate and their role in climate change. The treatment of aerosol properties and processes in regional and global models is becoming increasingly complex (Ackermann et al., 1998; Adams et al., 2001; Binkowski and Shankar, 1995; Binkowski and Roselle, 2003; Easter et al., 2004; Gong et al., 2003; Herzog et al., 2004; Jacobson, 2001; Lauer et al., 2005; Riemer et al., 2003; Stier et al., 2005; Wilson et al., 2001; Wright et al., 2000, 2001; Yu et al., 2003), taking into account more detailed microphysical and chemical interactions that underlie the formation of aerosol particles which then impact the climate system. More detailed representations of key aerosol properties such as size distributions, chemical composition (e.g., internal vs. external mixtures), hygroscopicity, optical properties, and cloud activation are also being incorporated into global climate models. With this increased level of detail, the question arises as to which method is most appropriate.

10 The most common methods of including aerosol size distributions and aerosol mixing information into models are the sectional, modal, and moment based schemes. Sectional models (Adams et al., 2001; Gong et al., 2003; Jacobson, 2001), which divide the size domain into intervals, or bins, calculate the evolution of the number concentrations in each size bin. This method has the disadvantage of being computationally expensive, because of the large number of bins required to accurately represent size and chemical mixing information. The modal method (Wilson et al., 2001; Iversen, 2002; Stier et al., 2005) approximates the size distribution by an assumed statistical function, most commonly multiple lognormal functions. The quadrature method of moments (QMOM) (McGraw, 1997) provides a computationally efficient statistically-based alternative to modal and sectional methods for aerosol simulation, that does not make a priori assumptions about the shape of the size distribution. Numerous modules based on the flexible and efficient moments method tracking 2–6 moments have been implemented into three-dimensional transport models (Ackermann et al., 1998; Binkowski and Shankar, 1995; Binkowski and Roselle, 2003; Easter et al., 2004; Herzog et al., 2004; Riemer et al., 2003; Wright et al., 2000, 2001; Yu et al., 2003). According to the theoretical framework, key moments of the aerosol population (such as number and

MATRIX

S. E. Bauer et al.

Title Page

Abstract

Introduction

Conclusions

References

Tables

Figures

I◀

▶I

◀

▶

Back

Close

Full Screen / Esc

Printer-friendly Version

Interactive Discussion



mass) that enter the covariance matrix of a principal component analysis are tracked instead of the distribution itself. The approach is flexible and highly efficient, yet can provide comprehensive representation of natural and anthropogenic aerosols and their mixing states.

5 Until recently aerosols in the GISS climate model (Schmidt et al., 2006) were treated in a mass-based scheme, in which the life cycles of sulfate, nitrate, black and organic carbon, sea salt, and dust were relatively independent from each other, except for surface reactions on mineral dust (Bauer and Koch, 2005; Bauer et al., 2007; Koch et al., 2006; Miller et al., 2006). Size information was included only for dust and sea salt
10 (using a bin scheme). For other species, size distributions were specified, number concentrations were not calculated, and water uptake effects were parameterized to depend upon relative humidity in the radiation and gravitational settling schemes. The implementation of MATRIX into the climate model will provide detailed aerosol characterization for formation, removal, and climate interactions to be calculated. In the
15 current module each of several aerosol modes is treated by a two-moment method, in which a set of mass and number concentrations is evolved. Efficient solvers based on analytic solutions to the moment equations are available (Binkowski and Roselle, 2003). This two-moment method is free of the concerns with moment consistency associated with larger moment sets, as number and mass concentrations are mathematically independent (unlike sets of three or more moments per mode), and solver
20 errors cannot generate inconsistent moment sets (Wright, 2007).

The goal of this paper is to give a complete model description of the microphysical model MATRIX (Sect. 2), present applications of MATRIX as a box model (Sect. 3), and as part of the GISS global climate model (Sect. 4). The MATRIX model provides a wide
25 set of possible model configurations of mode formulations and microphysical parameterizations. The full range of mode formulations will be discussed and tested in Sect. 3 with the box model. However, we will evaluate the model against field and station observations (Sect. 5) observations using one set of microphysical parameterizations. In a subsequent publication we will test the sensitivity of the global model performance for

MATRIX

S. E. Bauer et al.

Title Page

Abstract

Introduction

Conclusions

References

Tables

Figures

I◀

▶I

◀

▶

Back

Close

Full Screen / Esc

Printer-friendly Version

Interactive Discussion



several secondary particle formation schemes, thermodynamical modules, coagulation settings and mode formulations. Summary and conclusions are given in Sect. 6.

2 The microphysical model MATRIX

MATRIX aims at an intermediate degree of detail, completeness, and computational burden, greater than that typical of models with a small number of two-moment modes, but less than that of a sectional representation of multiple aerosol populations.

One goal of the model is to provide the number concentration and particle size information characterizing soluble particles for the treatment of cloud drop activation. This requires a representation of internal and external aerosol mixing processes. For example, insoluble particles can become soluble by acquiring soluble inorganic coatings as a result of either condensation of soluble species or coagulation with populations containing soluble materials.

The total aerosol is represented by a user-selected set of distinct populations (or modes), along with a specification of the coagulation interaction between the modes, that we refer to as an “aerosol mechanism”. Each mode has a distinct composition or set of chemical components, independent of size. Modes may be primary (those that receive particle emissions), secondary (those formed by coagulation among primary modes or condensation of gaseous components onto primary modes); or the mixed mode including all aerosol constituents. When particles from two modes coagulate such that the resulting particle cannot be accommodated in one of the defined modes, the particle is placed into the mixed mode.

The aerosol species treated in the present study are sulfate, nitrate, ammonium, water, black carbon (BC), organic carbon (OC), mineral dust, and sea salt. Not all species are defined for each mode, but the four inorganic species SO_4^{-2} , NO_3^- , NH_4^+ , and H_2O are defined for all modes. Although the aerosol consists of particles with differing composition and arbitrary size, the particles are assumed to be internally mixed with respect to the ammonium/sulfate, nitrate/sulfate and water/sulfate such that ratios

Title Page

Abstract

Introduction

Conclusions

References

Tables

Figures

◀

▶

◀

▶

Back

Close

Full Screen / Esc

Printer-friendly Version

Interactive Discussion



MATRIX

S. E. Bauer et al.

Title Page

Abstract

Introduction

Conclusions

References

Tables

Figures

I◀

▶I

◀

▶

Back

Close

Full Screen / Esc

Printer-friendly Version

Interactive Discussion



of the amounts of these substances are the same for all modes and all particle sizes (except for the additional water uptake by sea salt due to NaCl). This approach greatly reduces the required number of transported variables. Sulfate is transported for each mode; however for ammonium, nitrate and aerosol water, only the total concentrations summed over all modes needs to be transported. The ammonium, nitrate and water concentrations scale with sulfate and hence the distribution of these species over modes is derived from the sulfate distribution. An aerosol equilibrium module is used for gas-particle partitioning of inorganic species (SO_4^{-2} , NO_3^- , NH_4^+ , Na^+ , Cl^- , H_2O). Aerosol liquid water is a transported variable so that deliquescence-crystallization hysteresis can be represented.

The module represents new particle formation, particle emissions, gas-particle mass transfer, incorporation of sulfate from cloud-phase chemistry into the various modes, condensational growth, and coagulation within and between modes. MATRIX can be compiled in a variety of alternative “configurations”, each defined with a different set of modes.

The module also includes multiple alternative parameterizations for processes with important uncertainties, especially secondary particle formation. There are also multiple options for calculation of coagulation coefficients, intermodal transfer between the Aitken and accumulation modes, and inorganic aerosol equilibrium models. This paper presents a version of the module in which mode i is transported as a set of mass concentrations (M_i, q) and a number concentration (N_i), which provides the total mass and number in a mode and yields a 2-moment-per-mode representation.

2.1 Aerosol mechanisms

The aerosol mechanisms presented here vary in the number, composition, and the interaction among the modes defined. Eight mechanisms are currently set up as summarized in Table 1 and 2. The design of these mechanisms follows in large part the sectional model of Jacobson (2002) (J02 hereinafter). All mechanisms include the total aerosol ammonium, total aerosol nitrate, and total aerosol water, in addition to the

species defined for individual modes.

Mechanism 1, the most complex mechanism, consists of 16 modes and requires 51 transported species. Table 1a and b present the modes, species, lognormal parameters, and coagulation interactions for the mechanism. Mechanism 1 has 9 primary modes that receive particles through particle emissions: Aitken mode sulfate particles (AKK; diameter less than $0.1\ \mu\text{m}$), accumulation mode sulfate (ACC; diameter greater than $0.1\ \mu\text{m}$), insoluble fine mineral dust (DD1) and coarse mineral dust (DD2), fine sea salt (SSA), coarse sea salt (SSC), organic carbon (OCC), insoluble black carbon (BC1) and mixed BC-OC (BOC). The transfer between aitken and accumulation modes is described in Sect. 2.7.

Among these modes, mode AKK also receives particles from secondary particle formation, mode BOC also receives particles through BC-OC coagulation, and mode ACC also receives particles through growth of particles in mode AKK. All other modes acquire particles only as receptor modes for particles formed through coagulation of other (donor) modes, or reclassification of particles from other modes as they become soluble through acquisition of inorganic coatings. All modes undergo condensational growth and self-coagulation, and all but the mixed mode (MXX) undergo loss due to hetero-coagulation with other modes. Modes BC1, BC2, and BC3 contain black carbon with different volume fractions of inorganic coating (set to 0–5%, 5–20%, and >20%, respectively). All (non-biomass burning) black carbon is emitted into the insoluble primary mode BC1. Biomass burning emissions are assumed to go into the BOC mode. Condensation of inorganics on BC1, BC2, and BC3, and coagulation among these three modes may increase the volume fraction inorganics in these modes. When BC1 (BC2) coagulates with BC2 (BC3), the resulting particles initially go into BC1 (BC2) since they may have insufficient coating for classification as BC2 (BC3). At the end of each time step, if the volume fraction of inorganics in BC1 (BC2) rises above 5% (20%), all BC1 (BC2) particles are moved to mode BC2 (BC3). Particles in mode BCS (BC-sulfate) are formed solely through coagulation of AKK or ACC with BC1, BC2, or BC3. The secondary modes DS1 (soluble dust accumulation mode) and DS2 (soluble

MATRIX

S. E. Bauer et al.

Title Page

Abstract

Introduction

Conclusions

References

Tables

Figures

◀

▶

◀

▶

Back

Close

Full Screen / Esc

Printer-friendly Version

Interactive Discussion



MATRIX

S. E. Bauer et al.

[Title Page](#)[Abstract](#)[Introduction](#)[Conclusions](#)[References](#)[Tables](#)[Figures](#)[◀](#)[▶](#)[◀](#)[▶](#)[Back](#)[Close](#)[Full Screen / Esc](#)[Printer-friendly Version](#)[Interactive Discussion](#)

dust coarse mode) represent soluble particles produced by condensation of inorganics onto DD1 (insoluble dust accumulation mode) and DD2 (insoluble dust coarse mode), respectively. Modes DD1 and DD2 can also acquire inorganics through coagulation with mode AKK or ACC. Particles are transferred from DD1 to DS1 or DD2 to DS2 when the volume fraction of inorganics in DD1 or DD2 exceeds a threshold (set to 5%). The secondary mode DBC (dust-BC) receives particles solely through coagulation of any of the modes DD1, DD2, DS1, DS2 with any of the modes BC1, BC2, BC3, BCS. The mixed mode MXX receives the more complex aerosol mixtures and grows as the total aerosol approaches an internally mixed state. The transported species for the sea salt modes are the mass concentrations of dry sea salt (treated as NaCl) and the total non-sea salt sulfate summed over both modes. The non-sea salt sulfate is apportioned between the SSA and SSC modes in proportion to the sea salt (NaCl) in each mode. Number concentrations are derived from mass concentrations using assumed lognormal distributions ($D_{g,N}$, $\sigma_{g,N}$) given in Table 1a.

Mechanism 2, which also consists of 16 modes and 51 transported species, differs from mechanism 1 only in omission of mode BC3 and inclusion of mode OCS (OC-sulfate) resulting from coagulation of mode OCC with mode AKK or ACC, analogous to mode BCS. Mechanism 3 consists of 13 modes and requires 41 transported species. It differs from mechanism 1 in that (1) modes BC3 and BCS are omitted and black carbon aerosols are represented only by modes BC1 (insoluble) and BC2 (soluble), and (2) mode DBC (mineral dust-BC) is omitted and these particles are now placed in the mixed mode MXX.

Mechanism 4 consists of 10 modes and requires 34 transported species, described in Table 2. It differs from mechanism 1 in the omissions of modes AKK, BC3, BCS, DBC, and BOC, and the use of a single mode for sea salt (SSS). Mechanisms 5–8 differ from mechanisms 1–4 only in the representation of mineral dust by one insoluble and one soluble mode only. The numbers of modes are 14, 14, 11, and 8, and the number of transported species are 45, 45, 35, and 28, respectively.

2.2 Equations for evolution of number and mass concentrations

Equations for number and mass concentrations for each mode must be solved. These equations are similar to those solved by the Community Multiscale Air Quality (CMAQ) chemical transport model as described in [Binkowski and Roselle \(2003\)](#). Secondary particle formation from gaseous precursors, condensational growth, all coagulation processes, and addition of sulfate formed by in-cloud oxidation are treated as a group without operator splitting. The partitioning of semi-volatiles between the gas- and particle-phases is done just prior to, and again subsequent to, the calculation of the primary dynamical processes just cited. Any reclassification of particles from one mode to another is done at the end of the time step. For the number concentration N_i of mode i

$$\frac{dN_i}{dt} = P_i - L_i \quad (1)$$

$$P_i = J_i + E_i^{\text{num}} + R_i = J_i + E_i^{\text{num}} + \sum_{k \neq 1} \sum_{l > k, l \neq i}^n d_{ikl} K_{kl}^{(0)} N_k N_l \equiv c_i \quad (2)$$

$$L_i = \frac{1}{2} K_{ii}^{(0)} N_i^2 + \left(\sum_{j \neq i}^n d_{ij} K_{ij}^{(0)} N_j \right) N_i \equiv a_i N_i^2 + b_i N_i \quad (3)$$

where P_i and L_i are the production and loss rates, J_i the secondary particle formation rate (to be distinguished from the nucleation rate below), E_i^{num} the number concentration emission rate, R_i the rate at which particles enter mode i due to coagulation among all other modes. $K_{kl}^{(0)}$ is the mode-average coagulation coefficient (defined in Sect. 2.6 and Appendix B) for modes i and j , there are n modes, d_{ikl} is unity if coagulation of mode k with mode l produces particles in mode i and zero otherwise; d_{ij} is unity if coagulation of mode j with mode i results in the removal of particles from mode i and zero otherwise. The coefficients a_i , b_i , and c_i are defined for convenience and

Title Page

Abstract

Introduction

Conclusions

References

Tables

Figures

◀

▶

◀

▶

Back

Close

Full Screen / Esc

Printer-friendly Version

Interactive Discussion



all subscripts are dropped in considering solutions to the resulting equation, which is solved for each mode.

$$\frac{dN}{dt} = c - aN^2 - bN \quad (4)$$

5 Analytic solutions are obtained by holding the coefficients constant over a time step $\Delta t = t - t_0$ and are expressed using the quantities

$$\delta = (b^2 + 4ac)^{1/2}, r_1 = \frac{2ac}{b + \delta}, r_2 = -\frac{b + \delta}{2}, \gamma = -\left(\frac{r_1 - aN(t_0)}{r_2 - aN(t_0)}\right) \quad (5)$$

For $c \neq 0$ the approximated solution of Eq. (4) is

$$N(t) = \frac{r_1 + r_2 \gamma \exp(-\delta t)}{a[1 + \gamma \exp(-\delta t)]} \quad (6)$$

For $c = 0$ and $b \neq 0$ the solution is

$$10 \quad N(t) = \frac{bN(t_0) \exp(-bt)}{b + aN(t_0)[1 - \exp(-bt)]} \quad (7)$$

and for $c = 0$ and $b = 0$ the solution is

$$N(t) = \frac{N(t_0)}{1 + aN(t_0)t} \quad (8)$$

where sign errors in Eqs. (7) and (8) have been corrected from [Binkowski and Roselle \(2003\)](#). For the mass concentration $Q_{i,q}$ of species q in mode i

$$15 \quad \frac{dQ_{i,q}}{dt} = P_{i,q} - L_{i,q} = P_{i,q} - f_i^{(3)} Q_{i,q} \quad (9)$$

Title Page

Abstract

Introduction

Conclusions

References

Tables

Figures

◀

▶

◀

▶

Back

Close

Full Screen / Esc

Printer-friendly Version

Interactive Discussion



where $P_{i,q}$ and $L_{i,q}$ are the production and loss rates and $f_i^{(3)}$ is defined through the second equality. Analytic solutions are again obtained by holding the coefficient constant over the time step. For $f_i^{(3)} \neq 0$ the solution is

$$Q_{i,q}(t) = \frac{P_{i,q}}{f_i^{(3)}} + \left[Q_{i,q}(t_0) - \frac{P_{i,q}}{f_i^{(3)}} \right] \exp(-f_i^{(3)}t) \quad (10)$$

5 and for $f_i^{(3)} = 0$ the solution by an Euler forward step is

$$Q_{i,q}(t) = Q_{i,q}(t_0) + P_{i,q} \Delta t \quad (11)$$

The mass concentration production and loss terms treated in the aerosol module are

$$P_{i,q} = P_{i,q}^{\text{emis}} + P_{i,q}^{\text{npf}} + P_{i,q}^{\text{coag}} + P_{i,q}^{\text{growth}} + P_{i,q}^{\text{cloud}} \quad (12)$$

$$L_{i,q} = L_{i,q}^{\text{coag}} + L_{i,q}^{\text{gas-particle}} \quad (13)$$

10 where terms are included for particle emissions, secondary particle formation, coagulation, growth due to condensation and other gas-particle mass transfer, and incorporation of sulfate produced by in-cloud oxidation. Each of these terms and those for number concentrations in Eqs. (2) and (3) is discussed in a following section.

2.3 Secondary particle formation

15 The secondary particle formation production term is

$$P_{i,q}^{\text{npf}} = J_{p,i} m_{i,q}^{\text{npf}} \quad (14)$$

where $m_{i,q}^{\text{npf}}$ is the mass of species q in a newly formed particle added to mode i , and $J_{p,i}$ is the new particle formation (NPF) rate, determined from and less than the nucleation rate J . Only mode AKK receives new secondary particles, and only sulfate

Title Page

Abstract

Introduction

Conclusions

References

Tables

Figures

◀

▶

◀

▶

Back

Close

Full Screen / Esc

Printer-friendly Version

Interactive Discussion



is directly acquired by mode AKK; water and ammonium uptake are determined by subsequent equilibrium calculations. The nucleation rate is the rate at which critical-sized clusters of ~ 1 nm diameter are formed. The NPF rate $J_{p,i}$ is usually defined as the rate at which particles at the minimum detectable size are formed and is thus a function of measurement techniques, but in the present context $J_{p,i}$ is the rate at which particles of a user-selected small ambient diameter D_{npf} (3–20 nm) enter the Aitken mode. Explicit representation of particle dynamics at sizes less than D_{npf} is avoided through parameterizations that convert the nucleation rate J to the NPF rate at size D_{npf} , or directly give a NPF rate derived from field observations without reference to a nucleation rate. This section describes the MATRIX NPF model, which contains several nucleation parameterizations. The following submodules of the NPF model are described in Appendix A: (A1) parameterizations to convert J to $J_{p,i}$ by implicitly treating the particle dynamics at sizes less than D_{npf} , (A2) calculation of the mass of sulfate in a newly formed particle, and (A3) calculation of the steady-state concentration $[\text{H}_2\text{SO}_4]_{\text{SS}}$ used in the nucleation and NPF parameterizations.

Five nucleation or direct NPF parameterizations are available, two for binary homogeneous nucleation of H_2SO_4 - H_2O (Jaecker-Voirol and Mirabel, 1989; Vehkamäki et al., 2002), one for ternary homogeneous nucleation of H_2SO_4 - NH_3 - H_2O (Napari et al., 2002), one for nucleation by ion-ion recombination (Turco et al., 1998), and one for formation of particles of 3-nm diameter derived from field observations (Eisele and McMurry, 1997). The ion-ion recombination mechanism is taken as independent of the homogeneous mechanisms, and the ion-ion recombination contribution to the total nucleation rate is optionally included or set equal to zero.

- The Jaecker-Voirol and Mirabel (1989) parameterization is based on classical binary nucleation theory with hydrates, presented graphically, and designed for simple interpolation in T and RH. Each plot of $\log J$ vs. $\log [\text{H}_2\text{SO}_4]$ for T=[223, 248, 273, 298, 323] K and RH=[20, 40, 60, 80, 100]% were scanned, digitized, and fit to low-order polynomials for multi-linear interpolation and extrapolation to 0% RH. The range of rates covered by these fits is 10^{-3} – $10^5 \text{ cm}^{-3} \text{ s}^{-1}$.

Title Page

Abstract

Introduction

Conclusions

References

Tables

Figures

◀

▶

◀

▶

Back

Close

Full Screen / Esc

Printer-friendly Version

Interactive Discussion



MATRIX

S. E. Bauer et al.

Title Page

Abstract

Introduction

Conclusions

References

Tables

Figures

◀

▶

◀

▶

Back

Close

Full Screen / Esc

Printer-friendly Version

Interactive Discussion



– The [Vehkamaki et al. \(2002\)](#) parameterization is also based on classical binary nucleation theory with hydrates. Valid for $T=230.15\text{--}305.15\text{ K}$ and extrapolation to 190 K , $\text{RH}=0.01\text{--}100\%$ and $[\text{H}_2\text{SO}_4]=10^4\text{--}10^{11}\text{ molecules/cm}^3$. The parameterization is limited to conditions for which $10^{-7}<J\text{ (cm}^{-3}\text{ s}^{-1})<10^{10}$ and the critical nucleus contains at least 4 molecules.

– The [Napari et al. \(2002\)](#) parameterization is based on classical ternary nucleation theory, involving H_2SO_4 , NH_3 and H_2O . It is valid for $T=240\text{--}300\text{ K}$, $\text{RH}=5\text{--}95\%$, $[\text{H}_2\text{SO}_4]=10^4\text{--}10^9\text{ molecules/cm}^3$ and $[\text{NH}_3]=0.1\text{--}100\text{ ppt}$. The parameterization is limited to conditions for which $10^{-5}<J\text{ (cm}^{-3}\text{ s}^{-1})<10^6$. For $[\text{NH}_3]>100\text{ ppt}$, J is calculated using $[\text{NH}_3]=100\text{ ppt}$.

– The [Turco et al. \(1998\)](#) parameterization for ion induced nucleation is

$$J=Q_i f_{i0} \left(\frac{[\text{H}_2\text{SO}_4]}{[\text{H}_2\text{SO}_4]_0} \right)^{n^*} \quad (15)$$

where Q_i is the local ionization (and recombination) rate, and f_{i0} is the fraction of stabilizing recombination events at a reference vapor concentration of $[\text{H}_2\text{SO}_4]_0$. Following [Turco et al. \(1998\)](#), we set $[\text{H}_2\text{SO}_4]_0$ to $5 \times 10^6\text{ cm}^{-3}$, n^* to 3, and f_{i0} to 1×10^{-3} . The ionization rate Q_i varies with altitude from $2\text{ cm}^{-3}\text{ s}^{-1}$ near the surface to $\sim 30\text{ cm}^{-3}\text{ s}^{-1}$ at $\sim 12\text{ km}$. The ionization rate is an upper limit on the nucleation rate. No lower limit is placed on this rate.

– The observations of [Eisele and McMurry \(1997\)](#) for the flux of particles through the size 3–4 nm diameter was fit to the form $J=K[\text{H}_2\text{SO}_4]^n$ with (n, K) given by $(1, 5.8 \times 10^{-13})$ for the lower curve of Figure 7 in ([Eisele and McMurry, 1997](#)), $(2, 3.5 \times 10^{-15})$ for the upper curve, and $(1.5, 3.7 \times 10^{-14})$ for a curve drawn intermediate between the two. There are no bounding limits on input concentrations or new particle formation rates.

The conversion of the nucleation rate into a NPF and the calculation of the sulfate mass in a newly formed particle is presented in Appendix A.

2.4 Condensational growth and gas-particle mass transfer

The total production rate (averaged over the time step) of species q in mode i due to condensation of nonvolatile species and subsequent gas-particle mass transfer due to equilibration of other species is given by

$$P_{i,q}^{\text{growth}} = P_{i,q}^{\text{kinetic}} + P_{i,q}^{\text{equil}} = h_i P_q^{\text{kinetic}} + P_{i,q}^{\text{equil}} \quad (16)$$

where $P_{i,q}^{\text{growth}}$ is the total production rate of species q in mode i averaged over the time step, P_q^{kinetic} represents species treated kinetically (H_2SO_4), $P_{i,q}^{\text{equil}}$ represents species for which equilibrium is assumed (H_2O , NH_3 , HNO_3), h_i is the fraction of the total H_2SO_4 condensation rate due to particles in mode i , and $P_{i,q}^{\text{kinetic}}$ is the total condensation rate of H_2SO_4 summed over all modes, calculated as

$$P_q^{\text{kinetic}} = \frac{|\Delta[\text{H}_2\text{SO}_4]_{\text{cond}}|}{\Delta t} = \frac{[\text{H}_2\text{SO}_4][1 - \exp(-k_c \Delta t)]}{\Delta t} \quad (17)$$

where k_c is the total condensation sink. The condensation sink is the first-order rate constant for loss of $[\text{H}_2\text{SO}_4]$ onto particle surfaces (Kulmala et al., 2001) and is obtained as $k_c = \sum_{i=1}^n k_{c,i}$ with $k_{c,i}$ the contribution of mode i . For each mode the calculation of $k_{c,i}$ is based upon a single particle size, the diameter of average mass $\bar{D}_{p,i}$, and an adjustment factor $\theta_i = \exp[-(In\sigma_{g,i})^2]$ to prevent excessive condensation due to the use of a monodisperse distribution of diameter $\bar{D}_{p,i}$ (Okuyama et al., 1988). For mode i

$$k_{c,i} = 2\pi D_{\text{diff}} \int D_p \beta(Kn, \alpha) n_i(D_p) dD_p \approx 2\pi \theta_i D_{\text{diff}} \bar{D}_{p,i} \beta(Kn, \alpha) N_i \quad (18)$$

where D_{diff} is the binary diffusion coefficient of H_2SO_4 in air, D_p is the particle diameter, $Kn = 2\lambda/D_p$ is the Knudsen number with λ the vapor (H_2SO_4) mean free path in air,

Title Page

Abstract

Introduction

Conclusions

References

Tables

Figures

◀

▶

◀

▶

Back

Close

Full Screen / Esc

Printer-friendly Version

Interactive Discussion



α the mass accommodation coefficient of H_2SO_4 , n_i the number size distribution of mode i , N_j the particle number concentration in mode i , and β the transition regime correction to the condensational mass flux (Seinfeld and Pandis, 1998), given by

$$\beta(Kn, \alpha) = \frac{1 + Kn}{1 + 0.377Kn + 1.33Kn(1 + Kn)/\alpha} \quad (19)$$

5 A particle density is needed for each mode to obtain the diameter of average mass and is calculated from $\rho = m/V$, where the volume concentration V is calculated as a sum of contributions for each chemical component based on the current mode composition. The condensation sink is implemented through lookup tables for $k_{c,i}/N_j$ as a function of particle diameter calculated at representative heights for each host model vertical
10 level and using the standard atmosphere to an appropriate characteristic temperature and pressure to calculate D_{diff} and λ . The condensation sink was calculated with the mass accommodation coefficient α for H_2SO_4 set to 0.86 (Hanson, 2005), $\alpha = 1$ and $\lambda = \lambda_{\text{air}}$.

2.4.1 Partitioning ($P_{i,q}^{\text{equil}}$) of semi-volatile species

15 Two thermodynamic modules are included in MATRIX. EQSAM (Metzger et al., 2002b,a, 2006) which is built upon a simplified non-iterative expression for the activity coefficients, is very efficient. ISORROPIA (Nenes et al., 1998) which is more accurate but has a greater computational burden. At each time step, the number concentrations and mass concentrations of sulfate, BC, OC, mineral dust, sea salt are passed to MATRIX for each mode, and also the total aerosol nitrate, ammonium, liquid water, $\text{NH}_3(\text{g})$ and $\text{HNO}_3(\text{g})$. An aerosol thermodynamic model is used to partition the total $[\text{NH}_3] + [\text{NH}_4^+]$ and total $[\text{HNO}_3] + [\text{NO}_3^-]$ between the gas and condensed phase, and to obtain the liquid aerosol water concentration.

25 Aerosol phase water concentrations are calculated in two parts: (1) the water associated with all aerosol phase sulfate, nitrate, ammonium, and mineral dust concentrations summed over all modes, omitting sea salt (treated as NaCl) concentrations, using

[Title Page](#)[Abstract](#)[Introduction](#)[Conclusions](#)[References](#)[Tables](#)[Figures](#)[◀](#)[▶](#)[◀](#)[▶](#)[Back](#)[Close](#)[Full Screen / Esc](#)[Printer-friendly Version](#)[Interactive Discussion](#)

either EQSAM or the ISORROPIA thermodynamic module, and (2) the water associated with sea salt. The water from step 1 is distributed over modes in proportion to mode sulfate concentration, whereas the water from step 2 is distributed over modes in proportion to their sea salt concentrations.

5 Water uptake by sea salt aerosol is calculated as follows. The assumption is made that the volume concentration of water (volume $H_2O(l)$ per unit volume of space) in sea salt aerosol is given by $V_{H_2O} = V - V_{NaCl}$, with V the total volume concentration of the wet sea salt and V_{NaCl} the volume concentration of dry sea salt. The water mass concentration $m_{H_2O} (\mu g_{H_2O} m^{-3})$ is then calculated from the total sea salt concentration
 10 $m_{NaCl} (\mu g_{NaCl} m^{-3})$ as

$$\begin{aligned}
 & m_{H_2O} (\mu g_{H_2O} m^{-3}) \\
 &= \rho_{H_2O} V_{H_2O} \\
 &= \rho_{H_2O} (V - V_{dry}) \\
 &= \rho_{H_2O} (\xi^3 V_{dry} - V_{dry}) \\
 15 &= \rho_{H_2O} V_{dry} (\xi^3 - 1) \\
 &= \rho_{H_2O} (m_{NaCl} / \rho_{NaCl}) (\xi^3 - 1) \\
 &= m_{NaCl} (\mu g_{NaCl} m^{-3}) \times (\rho_{H_2O} / \rho_{NaCl}) (\xi^3 - 1)
 \end{aligned}$$

with $\xi(RH) = r/r_{dry}$. This holds for the fractional relative humidity RHF above the crystallization value 0.45. The expression for ξ is $\xi(RHF) = c_{SS} [b_{SS} + 1 / (1 - RHF)]^{1/3}$ with
 20 ρ_{NaCl} the density of NaCl ($2.165 g cm^{-3}$) and with $c_{SS} = 1.08$ and $b_{SS} = 1.2$.

Hysteresis effects are represented by the treatment of [Ghan et al. \(2001\)](#). For RH between the crystallization and deliquescence RH, the total metastable aerosol water content (step 1 + step 2) is calculated. If the actual current aerosol water content is greater than half this value, the aerosol is taken to be wet and the equilibrium water

MATRIX

S. E. Bauer et al.

Title Page	
Abstract	Introduction
Conclusions	References
Tables	Figures
◀	▶
◀	▶
Back	Close
Full Screen / Esc	
Printer-friendly Version	
Interactive Discussion	



content is distributed over all modes in proportion to their sulfate and sea salt concentrations. Otherwise, the aerosol is taken to be dry. The RH-deliquescent point is set to a constant value of 80% (appropriate for ammonium sulfate, following [Ghan et al., 2001](#)). The critical RH is set to a constant value of 35% (appropriate for ammonium sulfate, following [Ghan et al., 2001](#)) for the hysteresis calculation. As the water associated specifically with sea salt is not a tracked variable, this treatment is for the aerosol phase water as a whole.

2.5 Incorporation of sulfate produced by in-cloud aqueous-phase oxidation

The sulfate produced by in-cloud oxidation of SO₂ is distributed over a selected set of modes such that each activating particle receives an equal portion of that sulfate:

$$P_{i,q}^{\text{cloud}} = \frac{\zeta_i N_i}{\sum \zeta_i N_i} \frac{\Delta[\text{H}_2\text{SO}_4]_{\text{cond}}}{\Delta t} \quad (20)$$

where ζ_i is the fraction of particles in mode i that activate to form cloud droplets, N_i the particle number concentration in mode i , and $\Delta[\text{H}_2\text{SO}_4]_{\text{cond}}$ is the concentration of sulfate produced in-cloud during the time step.

MATRIX provides the host model cloud modules with either the number concentration of soluble particles for each mode, an estimate of the number of activating particles based on constant activating fractions for each mode, or an estimate of the number of activating particles based on the aerosol activation parameterizations of [Abdul-Razzak and Ghan \(1998, 2000\)](#). For the number concentration of soluble particles, the modes treated soluble are selected by setting the soluble (or activating) fraction of particles κ_i for each mode. In this study the fraction was set to unity for modes ACC, DS1, DS2, BC2, BC3, BCS, OCS, SSA, SSC, SSS, and MXX, 0.7 for mode OCC, and zero for all other modes.

The droplet activation parameterizations of [Abdul-Razzak and Ghan \(1998, 2000\)](#) treat multimodal and multicomponent aerosols. This parameterization provides the activated fraction for the number and mass concentrations for each mode, based on

Title Page

Abstract

Introduction

Conclusions

References

Tables

Figures

◀

▶

◀

▶

Back

Close

Full Screen / Esc

Printer-friendly Version

Interactive Discussion



Title Page

Abstract

Introduction

Conclusions

References

Tables

Figures

◀

▶

◀

▶

Back

Close

Full Screen / Esc

Printer-friendly Version

Interactive Discussion



mode composition and the updraft velocity. The mode-average hygroscopicity parameters are key in this treatment. The composition of the soluble components of mineral dust is treated as in Ghan et al. (2001). Modes that are thought of as insoluble cores with soluble shells, such as the BC and dust modes, may have a small soluble mass fraction that is effective at enhancing activation, and bulk treatment of these parameterizations may underestimate this enhancement. All modes are included in the activation calculation and each mode may have a nonzero activated fraction. The number concentration of activating particles for each mode is saved for use in the cloud modules, where aqueous chemistry, scavenging of interstitial particles (due to Brownian diffusion of particles to droplets), collision-coalescence and evaporation, aerosol resuspension, and wet removal is calculated.

2.6 Coagulation

A derivation of the intermodal coagulation production terms $P_{i,q}^{\text{coag}}$ and loss terms $L_{i,q}^{\text{coag}}$ for the mass concentration of species q in mode i is given in Appendix B. The production terms are

$$P_{i,q}^{\text{coag}} = \sum_{k=1}^n \sum_{l>k}^n g_{ikl,q} K_{kl}^{(3)} N_k N_l [(1 - \delta_{ki}) m_{k,q} + (1 + \delta_{li}) m_{l,q}] \quad (21)$$

where $g_{ikl,q}$ is unity if coagulation between modes k and l adds species q to mode i and is zero otherwise, $K_{kl}^{(3)}$ is a mode-average coagulation coefficient (defined in the Appendix B), δ_{kl} is the Kronecker delta, and $m_{j,q}$ is the mean mass of species q per particle in mode j . Modes k and l are distinct modes, and mode i may be a third distinct mode or the same mode as k or l . The loss terms are

$$L_{i,q}^{\text{coag}} = \sum_{j \neq i}^n d_{ij} K_{ij}^{(3)} N_j N_i m_{i,q} = \left(\sum_{j \neq i}^n d_{ij} K_{ij}^{(3)} N_j \right) (N_i m_{i,q}) \equiv f_i^{(3)} Q_{i,q} \quad (22)$$

MATRIX

S. E. Bauer et al.

Title Page

Abstract

Introduction

Conclusions

References

Tables

Figures

◀

▶

◀

▶

Back

Close

Full Screen / Esc

Printer-friendly Version

Interactive Discussion



The coagulation coefficient K_{ij} is the sum of five contributions: Brownian coagulation, the convective Brownian diffusion enhancement, gravitational collection, turbulent inertial motion and turbulent shear. The kernels are described in Jacobson (2005), and the values shown in Fig. 15.7 of Jacobson (2005) were reproduced by the MATRIX model. The collision efficiency for the gravitational collection was taken from Eq. (12–78) of Pruppacher and Klett (1980). The dependence of K_{ij} on temperature and pressure was examined by calculating K_{ij} for all pairs of particle sizes for a set of diameters ranging from 0.003–30 μm at several values T and p . For temperatures of 288, 200, and 325 K at a pressure of 101325 Pa, the ratio $K_{ij}(200 \text{ K}) / K_{ij}(288 \text{ K})$ ranged from 0.60 to 1.4, and the ratio $K_{ij}(325 \text{ K}) / K_{ij}(288 \text{ K})$ ranged from 0.90 to 1.2, showing a rather weak temperature dependence for K_{ij} . The Brownian K_{ij} is proportional to the sum of particle diffusion coefficients and thus depends on the Cunningham slip-flow correction to those coefficients, the particle Knudsen numbers, the mean free path, and thus the ambient pressure. For pressures of 101325, 10132.5, and 1013.25 Pa at a temperature of 288 K, the ratio $K_{ij}(10132.5 \text{ Pa}) / K_{ij}(101325 \text{ Pa})$ ranged from 0.41 to 8.0, and the ratio $K_{ij}(1013.25 \text{ Pa}) / K_{ij}(101325 \text{ Pa})$ ranged from 0.29 to 46, showing a significant pressure dependence for K_{ij} . The T and p dependence on K_{ij} is included through lookup tables for the mode-average coagulation coefficients \bar{K}_{ij} with table dimensions for T , p , and each of the lognormal parameters $D_{g,i}$, $D_{g,j}$, $\sigma_{g,i}$, and $\sigma_{g,j}$ for modes i and j . Table temperatures were 200, 260, 325 K and pressures were 101325, 10132.5, and 1013.25 Pa. The $D_{g,i}$ and $D_{g,j}$ each spanned the interval [0.003, 30.0] μm with 81 evenly-spaced (log scale) values, and for $\sigma_{g,i}$ and $\sigma_{g,j}$ 1.6, 1.8, and 2.0. For each pair of coagulating modes, $\sigma_{g,i}$ and $\sigma_{g,j}$ are fixed, and T , p , $D_{g,i}$ and $D_{g,j}$ are each linearly interpolated from the tabulated values. Precise mass conservation is accomplished by rescaling all mass variables for a specie at the end of each time step as needed to remove minor inaccuracies in the approximate analytic solutions when large time steps are used. These inaccuracies disappear as the time step or coagulation rates are reduced.

2.7 Intermodal transfer of sulfate from the Aitken to the accumulation mode

As newly-formed particles grow by condensation and self-coagulation, the mean diameter of the Aitken (AKK) mode may approach that of the accumulation (ACC) mode. To prevent the AKK mode from becoming too broad and containing excessively large particles, particles are transferred to the ACC mode as the AKK mode diameter approaches that of the ACC mode. This can be done in MATRIX in one of three ways. The first method is to transfer the fraction F_{rac}

$$F_{\text{rac}} = \left[\frac{(D_{p,\text{AKK}} - D_{p,\text{AKK},\text{min}})}{(D_{p,\text{ACC}} - D_{p,\text{AKK},\text{min}})} \right]^p \quad (23)$$

from AKK to ACC during the time step, where $D_{p,\text{AKK}}$ is the diameter of mean mass of mode AKK, $D_{p,\text{AKK},\text{min}}$ is the minimum value of $D_{p,\text{AKK}}$ and is the pre-selected size at which newly-formed particles appear in the model (10–20 nm is a good choice for our model), and $D_{p,\text{ACC}}$ is the diameter of mean mass of mode ACC. The exponent p is an adjustable parameter in the range $2 \leq p \leq 6$; the larger its value, the more intermodal transfer is delayed until the AKK mode closely approaches the ACC mode in mean size. As long as mode AKK is near the size at which new particles are formed, there is essentially no transfer; if mode AKK has grown to the size of mode ACC, the two modes are fully merged and the AK mode is emptied and ready to receive freshly-formed particles. When there are modest differences in mean particle size between the two modes, the transfer is spread over several time steps. This approach meets the criteria given in Whitby et al. (2002) for a stable intermodal transfer scheme. The second method follows Wilson et al. (2001), which is equivalent to Binkowski and Roselle (2003) with the diameter of intersection replaced by the fixed diameter $(D_{gn\text{AKK}}, D_{gn\text{ACC}})^{1/2}$. The third method is that of Binkowski and Roselle (2003) without modification.

Title Page

Abstract

Introduction

Conclusions

References

Tables

Figures

◀

▶

◀

▶

Back

Close

Full Screen / Esc

Printer-friendly Version

Interactive Discussion



3 Box model results

To demonstrate some of the capabilities of MATRIX, first we examine it as a box model and compare it to discrete model results. The coagulation scheme is tested, followed by a sensitivity study on aerosol activation for Mechanisms 1–8. The following parameterizations were used: (1) the thermodynamic equilibrium model EQSAM (see Sect. 2.4), (2) the nucleation mechanism by Napari et al. (2002), including ion to ion recombination by Turco et al. (1998) (see Sect. 2.3) and conversion into NPF by Kerminen and Kulmala (2002) (see Appendix A1) and (3) mode transfer is treated by the fractional transfer method (Eq. 23) with $p=4$.

3.1 Box model experiments: coagulation

Several test cases are examined focusing on coagulation of donor modes A and B to produce a distinct receptor mode C. This process is symbolized by the key interaction $A+B \rightarrow C$, although there are six distinct interactions: $A+C \rightarrow C$, $B+C \rightarrow C$, $A+B \rightarrow C$, and self-coagulation within all three modes. In all cases a 24-h period was simulated with a 0.5 h time step, with the discrete model subdividing the time step as needed to avoid the attempt to remove more particles from grid point i than exist at point i . Initial lognormal distributions are indicated as $[N(\text{cm}^{-3}), D_g(\mu\text{m}), \sigma_g(1)]$.

Figure 1 shows results for number and mass concentrations $N(t)$ and $M(t)$ for the coagulation $\text{OCC}+\text{BC1} \rightarrow \text{BOC}$. Initial distributions for the donor modes were identical with $[10^3, 0.053, 1.8]$. Both $N(t)$ and $M(t)$ were accurately predicted for all three modes. Figure 2 shows results for $\text{AKK}+\text{BC1} \rightarrow \text{BCS}$ where the initial distributions were $[10^4, 0.026, 1.6]$ for AKK and $[10^3, 0.053, 1.8]$ for BC1. Even though both $N(t)$ and $M(t)$ changed considerably more than in Fig. 1, the results were again quite accurate; the number of sulfate-coated BC particles was very accurately predicted.

Title Page

Abstract

Introduction

Conclusions

References

Tables

Figures

◀

▶

◀

▶

Back

Close

Full Screen / Esc

Printer-friendly Version

Interactive Discussion



3.2 Box model experiments: aerosol activation and mode configuration

Aerosol activation is also illustrated for each of the eight mechanisms described in Section 2. Initial number concentrations $N(\text{cm}^{-3})$ were AKK (2000), ACC (200), DD1 (10), DD2 (1), SSA (20), SSC (0.08), BC1 (1000), OCC (1000), and initial mass concentrations $M(\mu\text{g m}^{-3})$ were sulfate (0.913), BC (0.627), OC (0.369), dust (6.53), sea salt (7.16), ammonium (0.343). The production rates of gas-phase H_2SO_4 and aqueous sulfate were both set to $0.18 \mu\text{g m}^{-3} \text{h}^{-1}$, and the NH_3 source rate was set to two moles ammonia per mole sulfate. A fixed updraft velocity was set to 0.5 m s^{-1} . Figure 3 shows that both at the initial time and 6 hours later, all mechanisms except 4 and 8 give very similar numbers of activated particles though the number of aerosol species tracked varies from 35 to 51; mechanisms 4 and 8 do not represent the smaller sulfate particles with a distinct Aitken mode. For all mechanisms except 4 and 8, the activated aerosol was comprised of all of the modes of SCC and DD2 (DS2 acquired no particles), 95% of mode SSA, two-thirds of mode ACC, 0.6% of mode AKK, and variable contributions from modes containing BC and OC. For mechanisms 1-3, the activating fraction of accumulation mode dust was smaller than that of mode ACC, but increased over the 6-h period as dust particles acquired sulfate. Particles remaining in mode BC1 acquired enough sulfate to yield a small activating fraction (0.0006 with mechanism 1) after 6 hours. When mode BCS was present it showed an activated fraction 30%; when absent there was greater population of mode BC2. The total particle number increased slightly due to a small amount of new particle formation. Mechanisms 5-8 do not represent distinct modes for accumulation and coarse mode dust, yet the total numbers of activating particles for these mechanisms was very similar to those for mechanisms 1-4; however, combining modes AKK and ACC to form a single sulfate mode (mechanisms 4 and 8) led to a significantly higher number of activated particles.

Title Page

Abstract

Introduction

Conclusions

References

Tables

Figures

◀

▶

◀

▶

Back

Close

Full Screen / Esc

Printer-friendly Version

Interactive Discussion



4 The global climate model

The Goddard Institute for Space Studies (GISS) General Circulation Model (GCM) climate modelE (Schmidt et al., 2006; Hansen et al., 2005) is used as the host model for the microphysical MATRIX scheme. The model is employed on a horizontal resolution of $4^\circ \times 5^\circ$ latitude by longitude and 23 vertical layers. The model uses a 30 min time step for all physics calculations. A complete model description is given by Schmidt et al. (2006).

4.1 Sulfate chemistry

The sulfate aerosol module is based on the earlier work of Koch et al. (1999) and Koch et al. (2006) and includes prognostic simulations of the mass distributions of DMS, MSA, SO_2 and sulfate and includes a semi-prognostic simulation of H_2O_2 , full details of which can be found in the work of Koch et al. (1999). Briefly, the H_2O_2 production rate is calculated using fields of hydroperoxy radical (HO_2) concentration and H_2O_2 is destroyed photochemically and by reaction with OH using fields of H_2O_2 photolysis rate and OH concentration. ModelE includes the option to run the sulfate and nitrate chemistry coupled (Bell et al., 2005; Bauer et al., 2007) to the tropospheric gas-phase chemistry scheme (Shindell et al., 2003). The sulfate chemistry scheme provides the aqueous sulfate production rate for liquid clouds and the H_2SO_4 concentration for the MATRIX scheme.

4.2 Emissions

The term $P_{i,q}^{\text{emis}}$ (see Sect. 2.2) is the mass concentration emission rate of species q into mode i . Number concentration emission rates E_i^{num} are derived from mass concentration emission rates assuming lognormal size distributions and particle densities. Lognormal parameters $D_{g,E}$ and $\sigma_{g,E}$ (Tables 1a) are derived from Table 2 of Easter et al. (2004), except for sea salt and dust particles, which use particle sizes appropriate

Title Page

Abstract

Introduction

Conclusions

References

Tables

Figures

◀

▶

◀

▶

Back

Close

Full Screen / Esc

Printer-friendly Version

Interactive Discussion



for the GISS interactive emission models.

The emissions of the natural aerosols sea salt , dimethylsulfide (DMS) (Koch et al., 2006) and mineral dust (Miller et al., 2006) are calculated interactively in the model, depending on surface wind speed and other surface conditions. Sea salt emissions are calculated for two size classes, appropriate for the SSC and SSA mode. Mineral dust emissions are calculated for 4 size bins, as described in (Miller et al., 2006), and are distributed into the DD1 and DD2 mode.

Most sulfur emissions are into gaseous phase sulfur dioxide (SO₂); we assume that 2.5% of the sulfur is emitted as sulfate particles. 99% of these direct sulfate emissions are assigned to the ACC mode, and 1% into the AKK mode. Industrial carbonaceous emissions are assigned to the BC1 and OCC mode, but carbonaceous emissions from biomass burning sources are assigned to the BOC mode.

Since here we wish to simulate present day climate, the trace gas SO₂ and ammonia (NH₃) (Bouwman et al., 1997) emissions are based on the anthropogenic emissions for 1995 from the Emissions Database for Global Atmospheric Research (EDGAR3.2) (Olivier and Berdowski, 2001). Black (BC) and organic carbon (OC) emissions are from Bond et al. (2004). Biomass burning emissions for BC and OC are from the Global Fire Emission Database (GFED) model by van der Werf et al. (2003). Natural OM emissions are assumed to be derived from terpene emissions (Guenther et al., 1995), with a 10% production rate.

4.3 Transport and removal

Tracers, heat and humidity are advected using the highly nondiffusive Quadratic Upstream Scheme (QUS) of Prather (1986), which uses nine subgrid-scale spatial moments as well as the mean within each grid box. This increases the effective resolution of the tracer field and allows the GISS model to produce reasonable climate fields with relatively coarse resolution.

Turbulent dry deposition is based on the resistance-in-series scheme described in Koch et al. (1999) and Chin et al. (1996). The scheme is coupled to the model boundary

Title Page

Abstract

Introduction

Conclusions

References

Tables

Figures

◀

▶

◀

▶

Back

Close

Full Screen / Esc

Printer-friendly Version

Interactive Discussion



layer scheme of the GCM and depends on the aerosol mode mean diameter. Gravitational settling depends on the aerosol mode mean diameter and density and accounts for the effects of RH on density and size. The wet deposition schemes of the GISS modelE are described in Koch et al. (1999, 2006). The model has two types of clouds, convective and stratiform clouds. Tracer treatment in clouds follows the cloud processes, so that tracers are transported, dissolved, evaporated, and scavenged (with cloud water autoconversion and by raindrop impaction beneath clouds). This parameterization requires information about aerosol size and solubility, which are calculated for each aerosol mode by MATRIX. The solubility per mode is calculated by using a volume weighted approach, depending on the chemical composition of the aerosol particles.

5 GCM simulations

The performance of MATRIX on the global scale is examined by comparing a simulation of the full MATRIX scheme (Mechanism 1) with a simulation that excludes the microphysical processes of nucleation, coagulation and condensation. This leads basically to a simulation where all aerosols stay externally mixed as emitted, except particles that are emitted as internal mixtures (i.e. BC and OC from biomass burning). We compare these extreme cases, detailed mixed modes and externally mixed modes, to observations.

As discussed in the previous chapters, MATRIX provides a wide choice of mode configurations and parameterizations. In Sect. 3 all eight mode configurations were tested with the box model. On the global scale now we examine Mechanism 1, the most complex mechanism, using the following parameterizations: (1) The thermodynamic equilibrium model EQSAM (see Sect. 2.4), (2) the nucleation mechanism by Napari et al. (2002), including ion to ion recombination by Turco et al. (1998) (see Sect. 2.3) and conversion into NPF by Kerminen and Kulmala (2002) (see Appendix A1) and (3) mode transfer is treated by the fractional transfer method (Eq. 23) with $p=4$. The GCM

Title Page

Abstract

Introduction

Conclusions

References

Tables

Figures

◀

▶

◀

▶

Back

Close

Full Screen / Esc

Printer-friendly Version

Interactive Discussion



is simulated for 6 years under current climate conditions, and the mean over the last 5 years of the simulations will be analyzed in the following sections.

5.1 Mass simulation

Two experiments are carried out to examine the impact of micro-physical processes on the overall aerosol simulation. The experiment including the most complex mechanism 1 (BASE) will be compared with an experiment using exactly the same model setup, but excluding the micro-physical processes of nucleation, condensation and coagulation (NO-MIC). The NO-MIC experiment basically represents a mass only scheme, where only those aerosol modes are populated that experience chemical production or emission. For the current mechanism that will lead to population of the following modes: ACC (will comprise all sulfate), BC1, BOC, OCC, DD1, DD2, SSA and SSC. Fixed size and solubility is assumed for each mode. Note that for NO-MIC there is no means to render the insoluble modes (BC1, DD1, DD2) soluble.

Tables 3 and 4 present the budget per mass tracer and process for the BASE simulation. Figure 4 shows the annual mean column load concentrations per specie averaged over the last 5 years of the simulations.

Including micro-physical processes leads to a global increase of sulfate mass by 22% in the BASE simulation compared to the NO-MIC case. NO-MIC is lacking sulfate nucleation, condensation and coagulation processes. When those processes are neglected less sulfate mass is calculated, which would mainly come from nucleation and condensation (see Table 3). Nucleation adds small Aitken-mode particles into the atmosphere, leading to an overall longer lifetime of sulfate mass. This explains why the changes mainly occur in remote regions. Freshly nucleated particles tend to be engaged in the coagulation and condensation processes, which leads to a wide spread of sulfate material over aerosol mode and size ranges.

The changes seen in the nitrate concentrations simply complement the sulfate changes. More sulfate in the BASE case leads to less nitrate, as sulfate and nitrate compete for available ammonia in the system. Nitrate is reduced by 30% in the BASE

Title Page

Abstract

Introduction

Conclusions

References

Tables

Figures

◀

▶

◀

▶

Back

Close

Full Screen / Esc

Printer-friendly Version

Interactive Discussion



simulation compared to the NO-MIC experiment.

Black and organic carbon mass concentrations decrease globally by 20% and 10% in BASE, respectively, compared to NO-MIC. In BASE the coagulation and condensation processes lead to an increase in particles size and solubility and therefore shorten the lifetime of carbonaceous material in the atmosphere. These effects are especially important for reducing concentrations in remote regions.

The dust load is increased by 5% in the BASE simulation. Including micro-physical processes, leads to decreases dust loads in remote areas and increases dust load close to the sources. The removal in remote regions is explained by the fact that aged dust has a higher solubility, and therefore has higher wet removal rates which shortens lifetime and travel distance. The increase in the source region occurs because dust in the MXX mode has a smaller mean particle size than the pure DD1 or DD2 modes, which leads to less dry removal, especially gravitational settling of the very large particles in the source regions.

The changes in sea salt mass concentrations are rather small. Sea salt mass increases by 6% without microphysics, again caused by the shift in size distribution. As number and mass are independent, the mean particle size is not constrained to appropriate or even physically reasonable values. Hence, these distributions of number mean diameter reveal model characteristics not to be taken for granted. For the coarse modes, MATRIX tends to transfer mass out of the DS2 and SSC modes too quickly, but not number, with a tendency to predict mean particle sizes that are too small. As the SSC (and SSA) mean particle dry masses are fixed (so that number can be prescribed for these modes), the mean diameter distributions are sharply peaked for these modes. However, for mode DS2, there is a large spread in mean diameter extending to rather small sizes. This is not seen in mode DD2 as the mean diameter of this mode is strongly influenced by emissions at a fixed mean particle size.

The evaluation of the mass concentrations for the BASE simulation is presented in Fig. 5, where the surface mass concentrations of nitrate, sulfate, black and organic carbon are compared to observations from the North American IMPROVE and the

Title Page

Abstract

Introduction

Conclusions

References

Tables

Figures

◀

▶

◀

▶

Back

Close

Full Screen / Esc

Printer-friendly Version

Interactive Discussion



MATRIX

S. E. Bauer et al.

[Title Page](#)[Abstract](#)[Introduction](#)[Conclusions](#)[References](#)[Tables](#)[Figures](#)[I◀](#)[▶I](#)[◀](#)[▶](#)[Back](#)[Close](#)[Full Screen / Esc](#)[Printer-friendly Version](#)[Interactive Discussion](#)

European EMEP network. Nitrate aerosol mass concentrations in the scatter plot show a poor correlation, which is partly caused by the high spatial fluctuation of nitrate mass concentrations within a grid box. The comparison plots on the regional maps, show that model nitrate tends to be too low in California, but reasonable elsewhere in the country.

The European nitrate concentrations tend to be overestimated in central Europe, but reasonable in the north and the south. Sulfate mass shows a good comparison to observations, the only weak area is the central United States, where observations show much lower concentrations than simulated. The scatter plot shows the slight tendency of the model to simulate too high sulfate mass concentrations in the United States and too low concentrations in Europe. Carbonaceous aerosols are reasonably well simulated, but the model shows the tendency to underestimate regions with low concentrations in the United States.

Comparing the NO-MIC simulation to the above discussed data sets in Europe and the United States (not shown), shows quite similar results as the BASE simulation; only sulfate shows a better comparison to the IMPROVE data sets in the BASE simulation. Micro-physical mixing processes (as excluded in NO-MIC) have stronger impacts on the remote atmosphere, which are not covered by the EMEP and IMPROVE networks.

Black carbon aircraft measurements using the SP2 instrument were performed during three campaigns: winter (February 2006) and summer (August 2007) campaigns in Costa Rica (Schwarz et al., 2008) and two flights over Houston Texas in November 2004 (Schwarz and et al., 2006). The comparisons between model and observations of black carbon mass vertical profiles are presented in Fig 6. The observed concentrations show a sharp gradient in concentrations between boundary layer (PBL) and free tropospheric air over Costa Rica. The model predicts good boundary layer heights, but underestimates BC in the PBL, especially in summer, and overpredicts BC in the free troposphere. Black carbon in Costa Rica mostly comes from biomass burning sources, which has large temporal variability. The model monthly average cannot capture the precise variability in the aircraft observations. The overestimated BC concentrations

in the free troposphere over Costa Rica and Texas may be caused by inefficient cloud scavenging. The predominant aerosol mode in both regions is BOC. In both cases OC dominates the mode fraction, making those particles hydroscopic. However this still does not lead to sufficient wet removal.

5 An interesting aspect of the BC aircraft measurements is that black carbon coatings were also detected. Schwarz and et al. (2006) present (see Schwarz and et al. (2006), Fig. 6) the number fractions of internally mixed BC particles, ranging from 0.2 to 0.8. As shown in Fig. 6 our simulation predicts as main aerosol mode BOC in both regions, Costa Rica and Texas. This would translate into an internally mixing fraction of 1. In
10 order to match the observed mixing fraction we would need much more pure BC, i.e. BC in the BC1 mode. To investigate the simulated BC mixing states, we performed two sensitivity studies. (1) As discussed in the previous sections, BC and OC from biomass burning sources are directly assigned into the BOC mode. A test run was performed where all BC and OC is emitted as external mixture, to the modes BC1 and
15 OCC. However the results of this experiment looked virtually identical to the original experiment because the particles mix rapidly. (2) Again BC and OC emissions are treated as an external mixture, but the sizes of the emitted OC and BC particles were doubled. The results of this test are presented in Fig. 7. Total BC mass concentrations remain very similar to the original experiment, but the predominant aerosol mode is now BCS. This demonstrates the importance of the emitted aerosol size distribution. The main mixing process among aerosols is coagulation, which strongly depends on
20 particle size. Shifting OC particles into a larger size class leads to less mixing of BC and OC.

25 Figure 8 shows the column load and zonal mean distribution of BC, as sum over all BC modes, for the BASE experiment, and the differences between BASE and Exp. 2. On a global averaged, BC mass is decreased by 10% in Exp. 2. A decrease of BC mass is simulated all over the Northern Hemisphere and is most pronounced over Eastern Asia. In the BASE case, most BC is mixed with OC, whereas in Exp. 2 most BC is located in the BCS mode, therefore predominately mixed with sulfate. The shift

MATRIX

S. E. Bauer et al.

[Title Page](#)[Abstract](#)[Introduction](#)[Conclusions](#)[References](#)[Tables](#)[Figures](#)[I◀](#)[▶I](#)[◀](#)[▶](#)[Back](#)[Close](#)[Full Screen / Esc](#)[Printer-friendly Version](#)[Interactive Discussion](#)

of BC form the BOC into the BCS mode, leads to a longer lifetime of particles in the BOC mode (from 5.2 (BASE) to 6 (Exp. 2) days) and a shortened lifetime of the BCS mode (from 5.4 (BASE) to 4.2 (Exp. 2) days), which consequently leads to lower BC concentrations in sulfate rich areas, like for example East Asia. However, the changes in total BC mass are very small over Costa Rica and small over Houston Texas.

5.2 Number and size simulation

Aircraft observations from various campaigns (flight tracks are displayed in Fig. 9) and station data from aerosol supersites of the Global Atmosphere Watch program (<http://wdca.jrc.it>), are used for the evaluation of modeled aerosol number and size distributions.

The PEM Tropics-B campaign [Raper et al. \(2001\)](#) took place over the South Pacific ocean in spring 1999. Aerosol size distributions were measured in 30 size bins by two aerosol probes on board the DC-8 plane. Aerosol number concentrations spanning from 0.1 to 3 μm particle diameters as measured by the PCASP, and for particles of diameters between 0.34 and 20 μm by the FSSP aerosol probe. In order to compare those observations with the model, model data are interpolated to the flight tracks and monthly mean vertical profiles are calculated. Figure 10 shows the modeled and observed data for fine and coarse mode aerosols and indicates the simulated contributions from the individual modes to the total aerosol number concentration.

The differences between the two aerosol probes are quite large. The model simulation falls between the two measurements for particles sizes smaller than 1 μm . Here most particles come from the AKK, followed by the ACC, OCC, BOC and BCS modes. Close to the surface, the coated black carbon modes BC1, BC2 and BC3 show some small contribution to the total number concentration. Sulfate, nitrate and ammonium are the dominant species in this distribution, as they populate the AKK and ACC mode. The two aerosol probes show very different number concentrations for particle larger than 1 μm . However the model underestimates the number concentrations of those larger particles, which mainly come from the MXX and SSA modes.

Title Page

Abstract

Introduction

Conclusions

References

Tables

Figures

◀

▶

◀

▶

Back

Close

Full Screen / Esc

Printer-friendly Version

Interactive Discussion



MATRIX

S. E. Bauer et al.

[Title Page](#)[Abstract](#)[Introduction](#)[Conclusions](#)[References](#)[Tables](#)[Figures](#)[◀](#)[▶](#)[◀](#)[▶](#)[Back](#)[Close](#)[Full Screen / Esc](#)[Printer-friendly Version](#)[Interactive Discussion](#)

The TRACE-P [Jacob et al. \(2003\)](#) campaign took place from February to April in 2001 over the North Pacific ocean. Vertical profiles of mass and number concentrations are shown in [Fig. 11](#) and [12](#) as measured on the DC-8. In February the air craft flew between 150E and the US West coast sampling much cleaner air than during March and April, when Asian pollution dominated the shown profiles. [Figure 11](#) shows an excellent comparison between modelled and observed SO₂ and a good comparison to sulfate mass concentrations. Nitrate and ammonia tend to be underestimated by the model. The measurement data show the same order of magnitude of sulfate and nitrate concentrations in the polluted profiles during March. Number size distributions during TRACE-P were measured in six size bins, spanning from 0.1 to 1550 μm. Number concentration of particles lower than 1 μm are simulated reasonably well by the model (see [Fig. 12](#)) and the aerosol number concentrations in the coarse mode are underestimated. The precedence of modes is the same as over the South Pacific as seen from the comparisons to the PEM-Tropics-B campaign.

The campaigns discussed so far mainly sampled marine air masses. In contrast, the INTEX-A ([Singh et al., 2006](#)) campaign took place over the North American continent and to a smaller extent over the North Atlantic and Pacific Oceans. The mass observations ([Fig. 13](#)) show a good simulation of nitrate close to the surface, but lack of modelled nitrate at higher altitudes. Model sulfate aerosol mass seems reasonable in the lower atmosphere, but overestimated in higher levels. The comparison to number concentrations shows good agreement for particles lower than 2 μm and a lack of particles in the coarse mode, especially in the free troposphere. Observations are given in six size bins spanning from 0.3 to 2 μm. For these conditions, different modes are important. The BOC mode clearly dominates, followed by OCC and ACC in the boundary layer and the MXX mode in the free troposphere. The coarse mode shows again mostly contributions from SSC and MXX.

Station measurements provide the unique possibility to compare model data to long-term observations. Unfortunately only few data sets providing detailed particle size resolution are available. Here we show comparisons to three European stations, pro-

vided by the Global Atmosphere Watch program (<http://wdca.jrc.it/>).

Hohenpeißenberg is a mountain station at 988 m altitude located in southern Germany. Aerosol size distributions were measured from 0.1 to 6 μm . The year to year variability is very low, therefore we only compare data to the year 2002, as this was the most complete data set available. Figure 15 shows the annual mean size distribution as observed at Hohenpeißenberg. The model data are interpolated into the observed size bins. The smallest size bin starts at 0.1 μm . That is the bin in which the highest number concentrations are observed, however even higher concentration might occur at smaller particle sizes. The model captures the size distribution fairly well, but over-predicts the number concentration of particles greater than 1 μm . The two graphs in the top panel of Fig. 15 show us the mode and species contributions to this distribution. Particles smaller than 1 μm come from the AKK, and the coated black carbon modes (BC1,BC2,BC3). Dominating chemical species are sulfate and nitrate for the aiten mode particles and black carbon for particles around 0.05 μm size. The part of the size distribution that is observed and agrees well with the model, particle sizes 0.1 to 1 μm , have contributions from OCC, BOC, BCS and ACC, and to a limited extent contributions from the dust modes DS1 and DBC. The dominating chemical species in this part of the size distribution are sulfate, nitrate, organic and black carbon. Particles larger than 1 μm belong to the mixed mode MXX, and comprise dust, sea salt mixed with sulfate and nitrate.

Pallas is a station located in northern Finland, at 560 m altitude. Size distribution measurements are available from 0.007 to 0.4 μm (see Fig. 15). The model captures the number concentrations at the lower end of the size spectrum. Those particles get formed through nucleation events, belong to the AKK mode and are comprised mostly of sulfate and nitrate. Particle number concentrations of around 0.05 μm size are under-predicted by the model, which is primarily black carbon, and model and observations again agree pretty well for particles above 0.07 μm . Furthermore, the decreasing slope of the size distribution is captured by the model.

Ålesund is located in Spitzbergen, even further north of the Finish station Pallas.

Title Page

Abstract

Introduction

Conclusions

References

Tables

Figures

◀

▶

◀

▶

Back

Close

Full Screen / Esc

Printer-friendly Version

Interactive Discussion



The observations show somewhat smaller number concentrations in the nucleation mode, but a maximum in the distribution around $0.2 \mu\text{m}$. The model underestimates the number concentrations at this remote station, where black carbon, sulfate and nitrate dominate the size distribution below $0.1 \mu\text{m}$. Above that size organic carbon is present, and the agreement to observations is much improved.

Figure 16 presents the comparison of the three stations with model results from Exp. 2, where OC and BC emission sizes were doubled. It is very interesting to see how the prior visible gap in Fig. 15 around $1 \mu\text{m}$ particle sizes is now closed, at the expense of underestimating particles around $0.1 \mu\text{m}$.

5.3 Summary of GCM results

MATRIX has been successfully implemented into the GISS climate model and all 8 MATRIX mechanisms (see Sect. 2.) are functional in the global model. Although not shown here, the performances of mechanisms 1–4 show comparable results as the box model study. Especially the lag of the aitken mode AKK in mechanism 4 leads to significant changes in the overall model performance. Compressing the dust modes as done in mechanism 5–8 further leads to a decrease in accuracy in the coarse mode model performance. Therefore from the global point of view mechanisms 1–3 are useful options for global applications, although model modes need further optimization.

The novelty of MATRIX is adding aerosol number, size and mixing to the mass concentrations in the GISS climate model. The strengths and weaknesses of the MATRIX application on the global scale can be summarized as follows:

- Aerosol size distributions are well represented by the model for Aitken and accumulation mode particle sizes. This was demonstrated by the comparisons to aircraft as well as the station observations. The evaluation of aerosol size and number concentrations demonstrated a very successful simulation regarding number concentrations, below $1 \mu\text{m}$.
- Coarse mode particles are under-represented in the marine environment. Coarse

Title Page

Abstract

Introduction

Conclusions

References

Tables

Figures

◀

▶

◀

▶

Back

Close

Full Screen / Esc

Printer-friendly Version

Interactive Discussion



MATRIX

S. E. Bauer et al.

[Title Page](#)[Abstract](#)[Introduction](#)[Conclusions](#)[References](#)[Tables](#)[Figures](#)[◀](#)[▶](#)[◀](#)[▶](#)[Back](#)[Close](#)[Full Screen / Esc](#)[Printer-friendly Version](#)[Interactive Discussion](#)

mode aerosol data over land do not show this bias. This points to a lack of coarse sea salt aerosol in our model. Our model calculates sea salt emissions only for two size bins. This was sufficient for the mass based aerosol model version (Koch et al., 2006) of the GISS model, as only the small sea salt particles are important for the calculation of aerosol radiative forcing. However, coarse sea salt particles are important for aerosol mixing processes, as the coarse particles provide large surface areas for chemical and physical interaction. On the other hand the lifetime of coarse particles is very short, therefore their climate impact questionable.

- The most efficient process that leads to an internally mixed aerosol population is coagulation. Coagulation depends strongly on the size of the involved particles. However, there is limited information in emission inventories about the size of the emitted particles. This information is extremely important for the results of microphysical models.
- Testing the design of the MATRIX mode concept on the global scale showed that the definitions of the modes can still be optimized. Some modes are sparsely populated, for example the coated dust and black carbon modes, whereas fine aerosols tend to accumulate in the the BCS, the black organic carbon-sulfate mode and coarse mode aerosols accumulate in MXX, the mixed mode.
- Nitrate aerosols are calculated only as a mass based scheme, and the distribution over the modes is scaled relative to the sulfate distribution, as discussed in section 2. (The same concept applies for ammonium and aerosol water). Therefore the condensation of nitric acid on particles surfaces is not yet explicitly taken into account in the model formulation. This can lead to a lack of nitrate on coarse aerosol particles and explains the poor nitrate correlations in the remote atmosphere and higher altitudes, as demonstrated in Bauer et al. (2007); Bauer and Koch (2005).
- The sulfate mass simulation is improved by taking into account microphysical pro-

cesses. Furthermore sulfate material now spans the total size range of atmospheric particles. This will have an important impact on the calculation of the aerosol direct and indirect effects.

6 Conclusions

This manuscript gives a detailed description of the microphysical model MATRIX and also describes its performance as box and global models, as part of the GISS climate model. The climate model including MATRIX takes 6h computing time to simulate 1 model year, using 15 processors on a Linux Network cluster. Therefore this model system is very suitable to perform many sensitivity studies as well as perform transient climate simulations. MATRIX provides a wide set of possible mode configurations and microphysical parameterizations. It is beyond the scope of this first publication to present, analyze and evaluate all options of the MATRIX model. However, this paper gives the complete model description, which will serve as reference for all future studies. The MATRIX code is written as a box model and should be readily adaptable within other regional or global model frameworks. MATRIX is based on the quadrature method of moments (QMOM) scheme and the version presented in this paper includes two moments, number and mass, and one quadrature point. The two moment scheme was chosen as a starting point to develop the microphysical package, however our intention is to use higher aerosol moments in the future.

When designing a new model, decisions about what parameterizations to include or how to represent the aerosols will have large impacts on the end product, the impact of aerosols on the earth system. MATRIX tries to be as flexible as possible at this point, by including various sub-models, and allowing a wide variety of different mode configurations. The presented box model results demonstrated the large impact mode configuration can have on cloud activation. However the simulations on the global scale showed that some modes are sparsely populated, due to the tendency for aerosols to mix and to include more than two chemical components. For the Aitken and accumula-

Title Page

Abstract

Introduction

Conclusions

References

Tables

Figures

◀

▶

◀

▶

Back

Close

Full Screen / Esc

Printer-friendly Version

Interactive Discussion



tion mode particles, this leads to a dominance of the black, organic carbon and sulfate mixture, and in our formulation is allowed to include nitrate as well. In the coarse mode this favors the mixed mode, which allows all chemical species to be included in the aerosol. Our future work will focus on improving the simulation of aerosol mixtures, which will be an ongoing and difficult task. Detailed aerosol measurements are necessary to achieve this goal.

The coupling of the MATRIX aerosol schemes to radiation and cloud schemes is work under progress.

Appendix A

New particle formation

A1 Conversion of the nucleation rate to a NPF rate

The nucleation rate (or observed NPF rate at 3-nm diameter in the case of [Eisele and McMurry \(1997\)](#) is converted to a NPF rate at D_{npf} for all parameterizations. MATRIX is currently set up to use D_{npf} as either 3, 10, or 20 nm. Conversion is effected by the factor F in the expression $J_{p,i} = FJ$. Two approaches to F are available: (1) A simple mass-conservation approach with $F = [D_p^*(\text{nm})/D_{\text{npf}}(\text{nm})]^3$ conserves the total mass of sulfate in the nucleated particles, where D_p^* is 1 nm except for the [Eisele and McMurry \(1997\)](#) expression where it is 3 nm. (2) A more physically-based expression taking into account the small-particle dynamics (described) is the analytic formula for F is derived in [Kerminen and Kulmala \(2002\)](#) and [Kerminen et al. \(2004\)](#). It is given by

$$J_{p,i}(D_{\text{npf}}, t') = J(D_p^*, t) \exp\left(\frac{\eta}{D_{\text{npf}}} - \frac{\eta}{D_p^*}\right) \quad (\text{A1})$$

where the time t' at which the new particles appear and is later than the time t at which nucleation occurred on account of the time required for growth, and the parameter η

Title Page

Abstract

Introduction

Conclusions

References

Tables

Figures

◀

▶

◀

▶

Back

Close

Full Screen / Esc

Printer-friendly Version

Interactive Discussion



MATRIX

S. E. Bauer et al.

Title Page

Abstract

Introduction

Conclusions

References

Tables

Figures

◀

▶

◀

▶

Back

Close

Full Screen / Esc

Printer-friendly Version

Interactive Discussion



(nm) is calculated as $\gamma k_{c,\alpha=1}/4\pi g_r D_{\text{H}_2\text{SO}_4}$ with γ ($\text{nm}^2 \text{m}^2 \text{h}^{-1}$) a proportionality factor, $k_{c,\alpha=1}$ (s^{-1}) the condensation sink (see Eq. 18) calculated with the mass accommodation coefficient α set to unity and the mean free path of air (λ_{air}), g_d (nm h^{-1}) the diameter growth rate dD_p/dt , and $D_{\text{H}_2\text{SO}_4}$ ($\text{m}^2 \text{s}^{-1}$) the diffusivity of H_2SO_4 in air. The formula is applicable when the pre-existing aerosol and condensable vapor concentrations remain relatively constant during the time step and the total concentration of particles smaller than D_{npf} remains below 10^5 - 10^6cm^{-3} . The values of γ and g_d are assumed constant over a time step, and γ is a weakly varying function given by

$$\gamma = \gamma_0 \left[\frac{D_p^*}{1 \text{ nm}} \right]^{0.2} \left[\frac{D_{\text{npf}}}{3 \text{ nm}} \right]^{0.075} \left[\frac{D_{\text{mean}}}{150 \text{ nm}} \right]^{0.048} \left[\frac{\rho^*}{1000 \text{ kg m}^{-3}} \right]^{-0.33} \left[\frac{T}{293 \text{ K}} \right]^{-0.75} \quad (\text{A2})$$

where γ_0 is $0.23 \text{ nm}^2 \text{m}^2 \text{h}^{-1}$, D_{mean} (nm) is the number mean diameter of the pre-existing aerosol and ρ^* (kg m^{-3}) the density of the critical nucleus (set to 1.6 g cm^{-3}). Thus γ is nearly constant over the time step when these conditions are satisfied. If conditions are approximately steady-state, the difference in times t' and t is immaterial. Steady-state assumptions are discussed below. If η exceeds 56, F is set to 10^{-17} .

The diameter growth rate g_d of freshly nucleated particles is calculated as that due to condensation of inorganic vapors (H_2SO_4 , NH_3 , H_2O) only (contributions from low-volatility organic vapors in not yet represented) and is that of free molecular growth given by

$$g_d = \frac{dD_p}{dt} = \frac{\alpha}{2\rho} \bar{c} M_{\text{eff}} C$$

with α the mass accommodation coefficient of H_2SO_4 (taken as unity following Kerminen and Kulmala, 2002), ρ the density of such particles (set to 1.6 g cm^{-3}), \bar{c} the mean thermal velocity of an H_2SO_4 molecule, C the (steady-state) vapor concentration of H_2SO_4 , and M_{eff} is an effective molar mass for H_2SO_4 along with the NH_3 and H_2O that accompany it under the assumption of rapid equilibration

MATRIX

S. E. Bauer et al.

Title Page

Abstract

Introduction

Conclusions

References

Tables

Figures

◀

▶

◀

▶

Back

Close

Full Screen / Esc

Printer-friendly Version

Interactive Discussion



$$M_{\text{eff}} = M_{\text{H}_2\text{SO}_4} + n_{\text{NH}_3} M_{\text{NH}_3} + n_{\text{H}_2\text{O}} M_{\text{H}_2\text{O}}$$

where n_{NH_3} and $n_{\text{H}_2\text{O}}$ are the number of NH_3 and H_2O molecules condensing per H_2SO_4 molecule. For the number of NH_3 molecules per H_2SO_4 molecule condensing

$$n_{\text{NH}_3} = \frac{\text{flux of } \text{NH}_3 \text{ to particle}}{\text{flux of } \text{H}_2\text{SO}_4 \text{ to particle}} = \frac{\bar{c}_{\text{NH}_3}}{\bar{c}_{\text{H}_2\text{SO}_4}} \frac{C_{\text{NH}_3}}{C_{\text{H}_2\text{SO}_4}} = \left(\frac{M_{\text{H}_2\text{SO}_4}}{M_{\text{NH}_3}} \right)^{1/2} \frac{C_{\text{NH}_3}}{C_{\text{H}_2\text{SO}_4}}$$

5 with \bar{c}_i the mean thermal velocity of a molecule of type i , C_i the vapor number concentration of molecular species i , and with an upper bound of 2 imposed on n_{NH_3} . With n_{NH_3} determined, $n_{\text{H}_2\text{O}}$ is calculated by first treating the H_2SO_4 in the particles as either (a) H_2SO_4 for $n_{\text{NH}_3} < 0.5$, (b) NH_4HSO_4 for $0.5 \leq n_{\text{NH}_3} \leq 1.5$, or (c) $(\text{NH}_4)_2\text{SO}_4$ for $n_{\text{NH}_3} > 1.5$. The mole fraction sulfur in the particle χ_{S} is then defined as [mole S / (mole S + mole H_2O)]. For each neutralization state, polynomial fits for χ_{S} in terms of the fractional relative humidity h are used. The Kelvin effect reduces water uptake and its effect on χ_{S} is (optionally) included by replacing h with $h \exp(-2A/D_{\text{npf}})$ with A given by

$$A_{\text{H}_2\text{SO}_4} = [1.2 - 0.0072(T - 273.15)]$$

$$15 \quad A_{(\text{NH}_4)_2\text{SO}_4} = [1.2 - 0.0072(T - 273.15)] \times [1 - 0.17(1 - h)] \times [1 + 0.95(1 - h)]$$

and $A_{\text{NH}_4\text{HSO}_4}$ is the same as $A_{(\text{NH}_4)_2\text{SO}_4}$ on account of lack of data for ammonium bisulfate solutions. The first factor is due to the T dependence of surface tension of the solution (taken as that for water), the second factor is due to the dependence of the partial molar volume of water on h , and the third term is due to the dependence of the surface tension of the solution on h . Once χ_{S} is obtained, then $n_{\text{H}_2\text{O}} = (1 - \chi_{\text{S}}) / \chi_{\text{S}}$. Reference Lewis (2006).

A2 Calculation of the sulfate mass in a newly formed particle

The sulfate mass in a newly formed particle of ambient diameter D_{npf} as a function of RH and neutralization regime is now described. For each regime, and for D_{npf} selected as either 3, 10, or 20 nm, the diameter ratio $D_{\text{npf}}/D_{\text{npf}}$, dry is calculated from polynomial fits and used to convert the ambient particle volume ($\pi D_{\text{npf}}^3/6$) to dry particle volume, from which a sulfate (SO_4^{2-}) mass can be calculated (using appropriate densities and molecular weights for each regime). The Kelvin effect is taken into account. The calculated sulfate mass at a given RH is stored in a lookup table at increments of 1% RH for each regime.

Determination of the $[\text{H}_2\text{SO}_4]$ using in calculation of the nucleation rate and diameter growth rate g_d is now described. Operator splitting between gas-phase chemistry and aerosol microphysics is assumed, with the chemistry done prior to the aerosol processes. Accumulation of H_2SO_4 during the time step Δt of 0.5–2 h yields spuriously high initial H_2SO_4 concentrations for calculation of the nucleation rate directly from the initial $[\text{H}_2\text{SO}_4]$ and taking the total number of new particles formed as $J_{p,i} \Delta t$. Under suitable conditions, a steady-state H_2SO_4 concentration $[\text{H}_2\text{SO}_4]_{\text{SS}}$ can be derived from an estimate of its average production rate $P_{\text{H}_2\text{SO}_4}$ over the time step and its loss rate due to condensation on existing particles (the condensation sink) k_c . A time constant τ (s) is defined as $1/k_c$, and when $\Delta t \ll n_\tau \tau$ with n_τ a small integer (see below), the steady-state assumption is invoked, and an initial estimate of $[\text{H}_2\text{SO}_4]_{\text{SS}}$ is obtained as (Binkowski and Shankar, 1995)

$$[\text{H}_2\text{SO}_4]_{\text{SS}} = P_{\text{H}_2\text{SO}_4} / k_c = [\text{H}_2\text{SO}_4](\tau / \Delta t) \quad (\text{A3})$$

where the average production rate is based on the assumption that the sulfuric acid concentration at the beginning of the time step $[\text{H}_2\text{SO}_4]$ was produced by gas-phase chemistry during the current time step, which is perhaps a good approximation when significant production has occurred. Since $\tau \leq \Delta t$, $[\text{H}_2\text{SO}_4]_{\text{SS}}$ cannot not exceed $[\text{H}_2\text{SO}_4]$.

Title Page

Abstract

Introduction

Conclusions

References

Tables

Figures

◀

▶

◀

▶

Back

Close

Full Screen / Esc

Printer-friendly Version

Interactive Discussion



A3 Calculation of steady state concentrations

A further consideration arises under conditions for which very high nucleation rates would occur and consumption of H_2SO_4 by new particles formed during the time step cannot be neglected in determining the loss rate of H_2SO_4 . This is especially important with the ternary nucleation parameterization. A proper balance between consumption of H_2SO_4 by NPF and condensational growth is obtained by solving

$$\frac{d[\text{H}_2\text{SO}_4]}{dt} = P - k_c[\text{H}_2\text{SO}_4] - J_{p,i}([\text{H}_2\text{SO}_4])m_{q,i}^{\text{npf}} = 0 \quad (\text{A4})$$

at steady- state with the initial $[\text{H}_2\text{SO}_4]$ taken as $[\text{H}_2\text{SO}_4]_{\text{SS}}$ obtained from Eq. A3. The r.h.s. is positive with this value of $[\text{H}_2\text{SO}_4]$ as $J_{p,i} = FJ$ is always non-zero ($J_{p,i} \geq 10^{-24} \text{ cm}^{-3} \text{ s}^{-1}$). Equation A4 is then solved approximately by reducing $[\text{H}_2\text{SO}_4]$ by a factor of 1.1–1.5 until the r.h.s. becomes negative and $[\text{H}_2\text{SO}_4]_{\text{SS}}$ is then set to the final value. This provides a lower limit (within a factor of 1.1-1.5) for the actual $[\text{H}_2\text{SO}_4]_{\text{SS}}$ if Eq. A4 were solved exactly, and the slight underestimation of the $[\text{H}_2\text{SO}_4]_{\text{SS}}$ defined by Eq. A4 in part compensates for the neglect the loss of $[\text{H}_2\text{SO}_4]$ due to condensational growth of the new particles beyond D_{npf} during the time step. When k_c is small enough that $\tau > \Delta t$, the calculated initial $[\text{H}_2\text{SO}_4]_{\text{SS}}$ from Eq. A3 exceeds $[\text{H}_2\text{SO}_4]_0$ and the steady-state assumption cannot be invoked. For a time step of 0.5 h, k_c must be at least $5.6 \times 10^{-4} \text{ s}^{-1}$ to have $[\text{H}_2\text{SO}_4]_{\text{SS}} > [\text{H}_2\text{SO}_4]_0$. For a lognormal distribution with a number mean diameter of 150 nm and geometric standard deviation of 1.5, and taking $D_{\text{H}_2\text{SO}_4}$ as $1.0 \times 10^{-5} \text{ m}^2 \text{ s}^{-1}$, a number concentration of 88 cm^{-3} is required to yield a k_c value of $5.6 \times 10^{-4} \text{ s}^{-1}$ (derived from Table 1 of Kerminen and Kulmala (2002)). This is a significant amount of aerosol, and hence smaller aerosol loadings and values of k_c leading to $\tau > \Delta t$ will likely occur at a significant frequency in atmospheric models. When $\Delta t < n_\tau \tau$ the steady-state assumption is not invoked and the equation

$$\frac{d[\text{H}_2\text{SO}_4]}{dt} = P - k_c[\text{H}_2\text{SO}_4] \quad (\text{A5})$$

Title Page

Abstract

Introduction

Conclusions

References

Tables

Figures

◀

▶

◀

▶

Back

Close

Full Screen / Esc

Printer-friendly Version

Interactive Discussion



is solved to yield

$$[\text{H}_2\text{SO}_4](t) = [\text{H}_2\text{SO}_4]_0 e^{-k_c t} + \frac{Pt}{1 + k_c t} \quad (\text{A6})$$

where $[\text{H}_2\text{SO}_4]_0$ is the concentration at the beginning of the time step before gas-phase chemistry, and with the assumption that all H_2SO_4 present was generated by gas-phase chemistry during the current time step ($[\text{H}_2\text{SO}_4]_0 = 0$), the solution is

$$[\text{H}_2\text{SO}_4](t) = \frac{P}{k_c} \left(\frac{k_c t}{1 + k_c t} \right) = [\text{H}_2\text{SO}_4]_{\text{SS}} \left(\frac{1/\tau}{1 + t/\tau} \right) \quad (\text{A7})$$

and the H_2SO_4 concentration at the middle of the time step $[\text{H}_2\text{SO}_4]_{\Delta t/2}$ is given by

$$[\text{H}_2\text{SO}_4]_{\Delta t/2} = \frac{P}{k_c + 2/\Delta t} \quad (\text{A8})$$

and is used to calculate the nucleation rate and g_d . This expression neglects the consumption of H_2SO_4 through the formation of new particles and gives an upper limit for the actual $[\text{H}_2\text{SO}_4]_{\Delta t/2}$. Eq. A7 shows that for $t = \Delta t = n_\tau \tau$, $[\text{H}_2\text{SO}_4](t)$ is within $[100/(n_\tau + 1)]\%$ of its steady-state value when only production and condensation are considered, and since inclusion of NPF reduces τ and makes the approach to steady-state more rapid, the choice $n_\tau = 2$ leads to application of the steady-state approximation under conditions for which the sulfuric acid concentration will rise to within 33% of its steady-state value within the time step. For all values of τ , the NPF and condensational growth rates are first calculated independently using the initial concentration $[\text{H}_2\text{SO}_4]_0$ as if each process were permitted to consume all available H_2SO_4 . If the total H_2SO_4 consumed by the two processes exceeds $[\text{H}_2\text{SO}_4]_0$, the NPF and condensational growth rates are both reduced by the same factor such that the total H_2SO_4 consumption is limited to $[\text{H}_2\text{SO}_4]_0$. This favors a proper balance between consumption of H_2SO_4 by NPF and by condensational growth. For parity between these processes, the condensation rate is calculated from the same H_2SO_4 concentration described here to calculate the nucleation rate.

Title Page

Abstract

Introduction

Conclusions

References

Tables

Figures

◀

▶

◀

▶

Back

Close

Full Screen / Esc

Printer-friendly Version

Interactive Discussion



Appendix B

Derivation of production and loss terms for coagulation

For the coagulation of mode k with mode l to produce particle number or mass (or neither) in mode i , there are three cases. The first case occurs when $k=l=i$, which is self-coagulation within a single mode. The second case occurs when $k \neq l \neq i$, in which the distinct modes k and l coagulate to form a third distinct mode i . The third case occurs when either $k=i$ or $l=i$ (but not both) in which mass and number are lost from mode k or l and mass but not number is gained in mode i . Before discussing these cases, we define the mode-average coagulation coefficient or order n as

$$\bar{K}_{kl}^{(n)} = \frac{\int_0^\infty \int_0^\infty D_1^{(n)} K(D_1, D_2) n_k(D_1) n_l(D_2) dD_1 dD_2}{\int_0^\infty \int_0^\infty D_1^{(n)} n_k(D_1) n_l(D_2) dD_1 dD_2} \quad (\text{B1})$$

for number size distributions n_k and n_l for modes k and l , respectively, and particle diameters D_1 and D_2 . Note that for $n \neq 0$, $\bar{K}_{kl}^{(n)}$ is not symmetric in k and l , and for $n \neq 0$ the first index labels the donor mode (k or l) providing concentration of diameter moment n to the receiving mode (i).

The present model tracks number and mass concentrations only. The rate of change of number concentration N_i in mode i is expressed as production and loss terms as

$$\frac{dN_i}{dt} = P_{N,i}^{\text{coag}} - L_{N,i}^{\text{coag}} \quad (\text{B2})$$

and the rate of change of mass concentration $Q_{i,q}$ of species q in mode i is similarly expressed as

$$\frac{dQ_{i,q}}{dt} = P_{Q,N,i}^{\text{coag}} - L_{Q,N,i}^{\text{coag}} \quad (\text{B3})$$

Title Page

Abstract

Introduction

Conclusions

References

Tables

Figures

◀

▶

◀

▶

Back

Close

Full Screen / Esc

Printer-friendly Version

Interactive Discussion



Case 1: For the first case (self-coagulation), mass concentrations do not change and number concentration is reduced according to

$$L_{N,i}^{\text{coag}}(i+i \rightarrow i) = \frac{1}{2} \int_0^\infty \int_0^\infty K(D_1, D_2) n_i(D_1) n_i(D_2) dD_1 dD_2 = \frac{1}{2} \bar{K}_{ii}^{(0)} N_i^2 \quad (\text{B4})$$

Case 2: For the second case, mode k coagulates with mode l to add new particles and mass of species q to a mode i that is neither mode k nor mode l . Each coagulation event removes a particle from each of modes k and l and adds a particle to mode i . For the number concentration production rate in mode i

$$P_{N,i}^{\text{coag}}(k+l \rightarrow i) = \int_0^\infty \int_0^\infty K(D_1, D_2) n_k(D_1) n_l(D_2) dD_1 dD_2 = N_k N_l \bar{K}_{kl}^{(0)} \quad (\text{B5})$$

and the number concentration loss rate for mode k and mode l is also $L_{N,i}^{\text{coag}} = N_k N_l \bar{K}_{kl}^{(0)}$.

For the mass concentration of q , begin from the loss of third diameter moment (m^3 aerosol m^{-3} air) in mode k .

$$\frac{dM_{3,k}}{dt} = - \int_0^\infty \int_0^\infty D_1^{(3)} K(D_1, D_2) n_k(D_1) n_l(D_2) dD_1 dD_2 \quad (\text{B6})$$

The normalized third moment (m^3 aerosol per particle) for mode k can be expressed as

$$\bar{M}_{3,k} = \frac{\int_0^\infty \int_0^\infty D_1^{(3)} n_k(D_1) n_l(D_2) dD_1 dD_2}{\int_0^\infty \int_0^\infty n_k(D_1) n_l(D_2) dD_1 dD_2} = \frac{M_{3,k} N_l}{N_k N_l} \quad (\text{B7})$$

and combining Eqs. (A6) and (A7)

$$\frac{dM_{3,k}}{dt} = - N_k N_l \bar{M}_{3,k} \frac{\int_0^\infty \int_0^\infty D_1^{(3)} K(D_1, D_2) n_k(D_1) n_l(D_2) dD_1 dD_2}{\int_0^\infty \int_0^\infty D_1^{(3)} n_k(D_1) n_l(D_2) dD_1 dD_2} = - N_k N_l \bar{M}_{3,k} \bar{K}_{kl}^{(3)} \quad (\text{B8})$$

Title Page

Abstract

Introduction

Conclusions

References

Tables

Figures

◀

▶

◀

▶

Back

Close

Full Screen / Esc

Printer-friendly Version

Interactive Discussion



The mass concentration $Q_{k,q}$ of species q ($\mu\text{g } q \text{ m}^{-3}$ air) in mode k is related to the third moment as

$$Q_{k,q} = \rho_{k,q} V_k = \frac{\pi}{6} \rho_{k,q} M_{3,k} = \frac{\pi}{6} \left(\frac{m_{k,q}}{\frac{\pi}{6} \bar{M}_{3,k}} \right) M_{3,k} = \left(\frac{m_{k,q}}{\bar{M}_{3,k}} \right) M_{3,k} \quad (\text{B9})$$

with V_k the total aerosol volume concentration (m^3 aerosol m^{-3} air) of mode k , $\rho_{k,q}$ the mass of q per volume of particle ($\mu\text{g } q \text{ m}^{-3}$ aerosol), $m_{k,q}$ the average mass of q per particle ($\mu\text{g } q \text{ particle}^{-1}$) in mode k . In the parentheses following the third equality we have the ratio of units ($\mu\text{g } q \text{ particle}^{-1}$) / (m^3 aerosol particle^{-1}), which is ($\mu\text{g } q \text{ m}^{-3}$ aerosol) as required. Combining Eqs. (B8) and (B9), for the mass concentration loss of q in mode k

$$L_{Q,k,q}^{\text{coag}}(k + l \rightarrow i) = \frac{dQ_{k,q}}{dt} = - \frac{dM_{3,k}}{dt} \left(\frac{m_{k,q}}{\bar{M}_{3,k}} \right) = N_k N_l \bar{K}_{kl}^{(3)} m_{k,q} \quad (\text{B10})$$

and for likewise for mode l

$$L_{Q,l,q}^{\text{coag}}(k + l \rightarrow i) = \frac{dQ_{l,q}}{dt} = - \frac{dM_{3,l}}{dt} \left(\frac{m_{l,q}}{\bar{M}_{3,l}} \right) = N_k N_l \bar{K}_{kl}^{(3)} m_{l,q} \quad (\text{B11})$$

The production term for mode i then balances these losses

$$P_{Q,i,q}^{\text{coag}}(k + l \rightarrow i) = N_k N_l (\bar{K}_{kl}^{(3)} m_{k,q} + \bar{K}_{lk}^{(3)} m_{l,q}) \quad (\text{B12})$$

Case 3: For the third case, mode k (or l) coagulates with mode i , reducing number and mass concentrations in mode k and increasing the mass concentration of q (but not number concentration) in mode i . Each coagulation event removes a particle from mode k , and using previous results we have for the loss of number concentration in mode k

$$L_{N,k}^{\text{coag}}(k + i \rightarrow i) = N_k N_i \bar{K}_{ki}^{(0)} \quad (\text{B13})$$

Title Page

Abstract

Introduction

Conclusions

References

Tables

Figures

◀

▶

◀

▶

Back

Close

Full Screen / Esc

Printer-friendly Version

Interactive Discussion



and for the loss of mass concentration of q in mode k .

$$L_{Q,k,q}^{\text{coag}}(k+i \rightarrow i) = N_k N_i \bar{K}_{ki}^{(3)} m_{k,q} \quad (\text{B14})$$

For the mass production of q in mode i

$$P_{Q,i,q}^{\text{coag}}(k+i \rightarrow i) = N_k N_i \bar{K}_{ki}^{(3)} m_{k,q} \quad (\text{B15})$$

- 5 The expressions for production and loss rates obtained in these three cases are now combined and summed over modes as appropriate. For the production terms for number concentration in mode i , only the second case is nonzero, and summing over all pairs of modes k and l

$$P_{N,i,q}^{\text{coag}} = \sum_{k \neq i}^n \sum_{l > k, l \neq i}^n d_{ikl} K_{kl}^{(0)} N_k N_l \quad (\text{B16})$$

- 10 where d_{ikl} is unity if coagulation of modes k and l is defined to produce particles in mode i and zero otherwise, and there are n modes. Recall that in the second case mode i must be distinct from both k and l . The summand is symmetric in k and l , and the summation should include either $k > l$ or $l > k$, but not both. For the loss terms for number concentration, there is the self-coagulation term and all pairs of modes whose
- 15 intermodal coagulation results in the loss of particles from mode i

$$L_{N,i}^{\text{coag}} = \frac{1}{2} K_{ii}^{(0)} N_i^2 + \left(\sum_{j \neq i}^n d_{ij} K_{ij}^{(0)} N_j \right) N_i \quad (\text{B17})$$

where d_{ij} (not symmetric in i, j) is unity if coagulation of mode j with mode i results in the removal of particles from mode i and zero otherwise.

For the production terms for mass concentration of q in mode i , only in the second and third cases are nonzero and are combined as

$$P_{Q,i,q}^{\text{coag}}(k+l \rightarrow i, k+i \rightarrow i) = N_k N_l [(1 - \delta_{ki}) \bar{K}_{kl}^{(3)} m_{k,q} + (1 - \delta_{li}) \bar{K}_{lk}^{(3)} m_{l,q}] \quad (\text{B18})$$

Title Page

Abstract

Introduction

Conclusions

References

Tables

Figures

◀

▶

◀

▶

Back

Close

Full Screen / Esc

Printer-friendly Version

Interactive Discussion



MATRIX

S. E. Bauer et al.

Title Page

Abstract

Introduction

Conclusions

References

Tables

Figures

◀

▶

◀

▶

Back

Close

Full Screen / Esc

Printer-friendly Version

Interactive Discussion



where the Kronecker delta δ_{ki} ($\delta_{ki}=1$ for $k=i$, $\delta_{ki}=0$ for $k \neq i$) omits the k term since if $k=i$, mode k does not add mass to mode i , and similarly for δ_{ji} . For the first case above, $\delta_{ki} = \delta_{ji}=0$; for the second case, $\delta_{ki}=0$ and $\delta_{ji}=1$. Summing over all pairs of modes k and l , the production term for mode i is

$$P_{Q,i,q}^{\text{coag}} = \sum_{k=1}^n \sum_{l>k}^n g_{ikl,q} N_k N_l [(1 - \delta_{ki}) K_{kl}^{(3)} m_{k,q} + (1 - \delta_{li}) K_{lk}^{(3)} m_{l,q}] \quad (\text{B19})$$

where $g_{ikl,q}$ is unity if coagulation of modes k and l is defined as producing particles in mode i and either mode k or l is defined to contain species q ; it is zero if either of these conditions is not met. For the loss terms for mass concentration of q in mode i

$$L_{Q,i,q}^{\text{coag}} = \sum_{j \neq i}^n d_{ij} N_j N_i K_{ij}^{(3)} m_{i,q} = \left(\sum_{j \neq i}^n d_{ij} K_{ij}^{(3)} N_j \right) (N_i m_{i,q}) \equiv f_i^{(3)} Q_{i,q} \quad (\text{B20})$$

where d_{ij} (not symmetric in i, j) is unity if coagulation of mode j with mode i results in the removal of particles from mode i and zero otherwise (as defined above).

Acknowledgements. This work has been supported by the NASA MAP program Modeling, Analysis and Prediction Climate Variability and Change (NN-H-04-Z-YS-008-N), managed by Don Anderson. Observational data were obtained from the NASA Langley Research Center Atmospheric Science Data Center, the EMEP, IMPROVE and GAW network. We thank Joshua Schwarz for providing the aircraft measured black carbon data sets and his helpful discussions.

References

- Abdul-Razzak, H. and Ghan, S.: A parameterization of aerosol activation – 1. Single aerosol type, *J. Geophys. Res.*, 103 (D6), 6123–6131, 1998. [9947](#)
- Abdul-Razzak, H. and Ghan, S.: A Parameterization of Aerosol Activation. Part 2: Multiple Aerosol Types, *J. Geophys. Res.*, 105, 6837–6844, 2000. [9947](#)

MATRIX

S. E. Bauer et al.

Title Page

Abstract

Introduction

Conclusions

References

Tables

Figures

◀

▶

◀

▶

Back

Close

Full Screen / Esc

Printer-friendly Version

Interactive Discussion



- Ackermann, I. J., Hass, H., Memmesheimer, M., Ebel, A., Binkowski, F. S., and Shankar, U.: Modal aerosol dynamics model for Europe: Development and first applications, *Atmos. Environ.*, 32, 2981–2999, 1998. [9933](#)
- Adams, P. J., Seinfeld, J. H., Koch, D., Mickley, L., and Jacob, D.: General circulation model assessment of direct radiative forcing by the sulfate-nitrate-ammonium-water inorganic aerosol system, *J. Geophys. Res.*, 106, 1097–1112, doi:10.1029/2000JD900512, 2001. [9933](#)
- Bauer, S. E. and Koch, D.: Impact of Heterogeneous Sulfate Formation at Mineral Dust Surfaces on Aerosol Loads and Radiative Forcing in the GISS GCM, *J. Geophys. Res.*, 110, doi:10.1029/2005JD005870, 2005. [9934](#), [9964](#)
- Bauer, S. E., Mishchenko, M., Laciš, A., Zhang, S., Perlwitz, J., and Metzger, S.: Do Sulfate and Nitrate Coatings on Mineral Dust have Important Effects on Radiative Properties and Climate Modeling?, *J. Geophys. Res.*, 112, doi:10.1029/2005JD006977, 2007. [9934](#), [9953](#), [9964](#)
- Bell, N., Koch, D., and Shindell, D. T.: Impacts of Chemistry-Aerosol coupling on tropospheric ozone and sulfate simulations in a general circulation model, *J. Geophys. Res.*, 111, 2005. [9953](#)
- Binkowski, F. S. and Roselle, S.: Models-3 Community Multiscale Air Quality (CMAQ) model aerosol component 1. Model description., *J. Geophys. Res.*, 108, 2003. [9933](#), [9934](#), [9939](#), [9940](#), [9950](#)
- Binkowski, F. S. and Shankar, U.: Models-3 Community Multiscale Air Quality (CMAQ) model aerosol component 1. Model description, *J. Geophys. Res.*, 100, 26 191–26 209, 1995. [9933](#), [9969](#)
- Bond, T. C., Streets, D., Yarber, K., Nelson, S., Woo, J., and Klimont, Z.: A technology-based global inventory of black and organic carbon emissions from combustion, *J. Geophys. Res.*, 109, D14203, doi:10.1029/2003JD003697, 2004. [9954](#)
- Bouwman, A. F., Lee, D. S., Asman, W. A. H., Dentener, F. J., Hoek, K. W. V. D., and Olivier, J.: A Global High-Resolution Emission Inventory for Ammonia, *Global Biogeochemical Cycles*, 11, 561–587, 1997. [9954](#)
- Chin, M., M., D. J. J., Gardner, G. M., Foreman-Fowler, M. S., Spiro, P. A., and Savoie, D. L.: A global three-dimensional model of tropospheric sulfate, *J. Geophys. Res.*, 101, 18 667–18 690, 1996. [9954](#)
- Easter, R. C., Ghan, S. J., Zhang, Y., Saylor, R., Chapman, E., Laulainen, N., Abdul-Razzak, H., Leung, L., Bian, X., and Zaveri, R.: MIRAGE: Model description and evaluation of aerosols

MATRIX

S. E. Bauer et al.

Title Page

Abstract

Introduction

Conclusions

References

Tables

Figures



Back

Close

Full Screen / Esc

Printer-friendly Version

Interactive Discussion



- and trace gases, *J. Geophys. Res.*, 109, D20210, 2004. [9933](#), [9953](#)
- Eisele, F. L. and McMurry, P. H.: Recent progress in understanding particle nucleation and growth, *Phil. Trans. R. Soc. Lond. B*, 352, 191–201, 1997. [9942](#), [9943](#), [9966](#)
- Ghan, S. and Schwartz, S.: Aerosol properties and processes. A path from field and laboratory measurements to global climate models, *Bull. of the American Met. Soc.*, 8, 1059–1083, 2007. [9932](#)
- Ghan, S., Laulainen, N., Easter, R., Wagener, R., Nemesure, S., Chapman, E., Zhang, Y., and Leung, R.: Evaluation of aerosol direct radiative forcing in MIRAGE, *J. Geophys. Res.*, 106, 5295–5316, 2001. [9946](#), [9947](#), [9948](#)
- Gong, S. L., Barrie, L. A., Blanchet, J. P., von Salzen, K., Lohmann, U., Lesins, G., Spacek, L., Zhang, L. M., Girard, E., Lin, H., Leaitch, R., Leighton, H., Chylek, P., and Huang, P.: Canadian Aerosol Module: A size-segregated simulation of atmospheric aerosol processes for climate and air quality models, 1, Module development, *J. Geophys. Res.*, 108, 4007, doi:10.1029/2001JD002002, 2003. [9933](#)
- Guenther, A. B., Hewitt, N., Erickson, D., Fall, R., Geron, C., Graedel, T., Harley, P., Klinger, L., Lerdau, M., McKay, W. A., Pierce, T., Scholes, B., Steinbrecher, R., Tallamraju, R., Taylor, J., and Zimmerman, P.: A global model of natural volatile organic compound emissions, *J. Geophys. Res.*, 100, 8873–8892, 1995. [9954](#)
- Hansen, J., Sato, M., Ruedy, R., Nazarenko, L., Lacis, A., Schmidt, G., Russell, G., Aleinov, I., Bauer, M., Bauer, S., Bell, N., Cairns, B., Canuto, V., Cheng, Y., Genio, A. D., Faluvegi, G., Fleming, E., Friend, A., Hall, T., Jackman, C., Kelley, M., Kiang, N., Koch, D., Lean, J., Lerner, J., Lo, K., Menon, S., Miller, R., Minnis, P., Novakov, T., Oinas, V., Perlwitz, J., Perlwitz, J., Rind, D., Romanou, D., Shindell, D., Stone, P., Sun, S., Tausnev, N., Thresher, D., Wielicki, B., Wong, T., Yao, M., and Zhang, S.: Efficacy of Climate Forcing, *J. Geophys. Res.*, 110, D18104, doi:10.1029/2005JD005776, 2005. [9953](#)
- Hanson, D. R.: Mass accommodation of H₂SO₄ and CH₃SO₃H on water-sulfuric acid solutions from 6% to 97% RH, *J. Phys. Chem., A* 109, 6919–6927, 2005. [9945](#)
- Herzog, M., Weisenstein, D., and Penner, J.: A dynamic aerosol module for global chemical transport models: Model description, *J. Geophys. Res.*, 109, D18202, doi:10.1029/2003JD004405, 2004. [9933](#)
- Iversen, T.: A scheme for process-tagged SO₄ and BC aerosols in NCAR CCM3: Validation and sensitivity to cloud processes, *J. Geophys. Res.*, 107, 4751, doi:10.1029/2001JD000885, 2002. [9933](#)

MATRIX

S. E. Bauer et al.

Title Page

Abstract

Introduction

Conclusions

References

Tables

Figures

I◀

▶I

◀

▶

Back

Close

Full Screen / Esc

Printer-friendly Version

Interactive Discussion



- Jacob, D. J., Crawford, J., Kleb, M., Connors, V. S., Bendura, R. J., Raper, J. L., Sachse, G. W., Gille, J. C., Emmons, L., and Held, C. L.: Transport and chemical evolution over the Pacific (TRACE-P) aircraft mission: Design execution and first results, *J. Geophys. Res.*, 108(D20), 9000, doi:10.1029/2002JD003276, 2003. [9961](#)
- 5 Jacobson, M.: Analysis of aerosol interactions with numerical techniques for solving coagulation, nucleation, condensation, dissolution, and reversible chemistry among multiple size distributions, *J. Geophys. Res.*, 107(D19), 4366, doi:10.1029/2001JD002044, 2002. [9936](#)
- Jacobson, M.: *Fundamentals of Atmospheric Modeling*, Cambridge University Press, 2005. [9949](#)
- 10 Jacobson, M. Z.: Global direct radiative forcing due to multicomponent anthropogenic and natural aerosols, *J. Geophys. Res.*, 106, 1551–1568, 2001. [9933](#)
- Jaeger-Voirol, A. and Mirabel, P.: Heteromolecular nucleation in the sulfuric acid-water system, *J. Geophys. Res.*, 23, 2053–2057, 1989. [9942](#)
- Kerminen, V. M. and Kulmala, M.: Analytical formulae connecting the real and the apparent nucleation rate and the nuclei number concentration for atmospheric nucleation events, *Journal of Aerosol Science*, 33, 609–622, 2002. [9951](#), [9955](#), [9966](#), [9967](#), [9970](#)
- 15 Kerminen, V. M., Anttila, T., Lehtinen, K., and Kulmala, M.: Parameterization for atmospheric new-particle formation: Application to a system involving sulfuric acid and condensable water-soluble organic vapors, *Aerosol Science and Technology*, 38, 1001–1008, 2004. [9966](#)
- 20 Koch, D., Jacob, D., Tegen, I., Rind, D., and Chin, M.: Tropospheric sulfur simulation and sulfate direct radiative forcing in the Goddard Institute for Space Studies general circulation model, *J. Geophys. Res.*, 104, 23 799–23 822, 1999. [9953](#), [9954](#), [9955](#)
- Koch, D., Schmidt, G., and Field, C.: Sulfur, sea salt and radionuclide aerosols in the GISS modelE, *J. Geophys. Res.*, 111, D06206, doi:10.1029/2004JD005550, 2006. [9934](#), [9953](#), [9954](#), [9955](#), [9964](#)
- 25 Kulmala, M., Maso, M. D., Makela, J. M., Pirjola, L., Vakeva, M., Aalto, P., Miikkulainen, P., Hameri, K., and O’Dowd, C. D.: On the formation, growth and composition of nucleation mode particles, *Tellus*, 53B, 479–490, 2001. [9944](#)
- Lauer, A., Hendricks, J., Ackermann, I., Schell, B., Hass, H., and Metzger, S.: Simulating aerosol microphysics with the ECHAM/MADE GCM – Part I: Model description and comparison with observations, *Atmos. Chem. Phys.*, 5, 3251–3276, b2005. [9933](#)
- 30 Lewis, E. R.: The effect of surface tension (Kelvin effect) on the equilibrium radius of a hygroscopic aqueous aerosol particle, *J. Aerosol Sci.*, 37, 1605–1617, 2006. [9968](#)

MATRIX

S. E. Bauer et al.

Title Page

Abstract

Introduction

Conclusions

References

Tables

Figures

I◀

▶I

◀

▶

Back

Close

Full Screen / Esc

Printer-friendly Version

Interactive Discussion



- McGraw, R.: Description of aerosol dynamics by the quadrature method of moments, *Aerosol Science and Technology*, 27, 255–265, 1997. [9933](#)
- Metzger, S., Mihalopoulos, N., and Lelieveld, J.: Importance of mineral cations and organics in gas-aerosol partitioning of reactive nitrogen compounds: case study based on MINOS results, *Atmos. Chem. Phys.*, 2549–2567, 2006. [9945](#)
- Metzger, S. M., Dentener, F. J., Jeuken, A., Krol, M., and Lelieveld, J.: Gas/aerosol partitioning 2: Global model results, *J. Geophys. Res.*, 107, 2002a. [9945](#)
- Metzger, S. M., Dentener, F. J., Lelieveld, J., and Pandis, S. N.: Gas/aerosol partitioning 1: A computationally efficient model, *J. Geophys. Res.*, 107, 2002b. [9945](#)
- Miller, R. L., Cakmur, R., Perlwitz, J., Geogdzhayev, I., Ginoux, P., Kohfeld, K., Koch, D., Prigent, C., Ruedy, R., Schmidt, G., and Tegen, I.: Mineral dust aerosols in the NASA Goddard Institute for Space Sciences ModelE atmospheric general circulation model, *J. Geophys. Res.*, 111, D06208, doi:10.1029/2005JD005796, 2006. [9934](#), [9954](#)
- Napari, I., Noppel, M., Vehkamäki, H., and Kulmala, M.: Parametrization of ternary nucleation rate for H₂SO₄-NH₃-H₂O vapors, *J. Geophys. Res.*, 107(D19), 4381, doi:10.1029/2002JD002132, 2002. [9942](#), [9943](#), [9951](#), [9955](#)
- Nenes, A., Pilinis, C., and Pandis, S. N.: Isorropia: A new thermodynamic model for multiphase multicomponent inorganic aerosols, *Aquat. Geochem.*, pp. 123–152, 1998. [9945](#)
- Okuyama, K., Kousaka, Y., Kreidenweis, S., Flagan, R., and Seinfeld, J.: Studies in binary nucleation: the dibutylphthalate/dioctylphthalate system, *J. Chem. Phys.*, 89, 6442–6453, 1988. [9944](#)
- Olivier, J. and Berdowski, J.: Global emissions sources and sinks, chap. The climate System, pp. 33–78, ISBN 90 5809 255 0, Swets and Zeitlinger Publishers, Lisse, The Netherlands., 2001. [9954](#)
- Prather, M. J.: Numerical advection by conservation of second order moments., *J. Geophys. Res.*, 91, 6671–6680, 1986. [9954](#)
- Pruppacher, H. and Klett, J.: *Microphysics of Clouds and Precipitation*, D. Reidel Publishing Company, Dordrecht/Boston/London, 1980. [9949](#)
- Raper, J. L., Kleb, M., Jacob, D., and et al.: Pacific Exploratory Mission in the tropical Pacific: PEM-Tropics B, March–April 1999, *J. Geophys. Res.*, 32 401–32 425, 2001. [9960](#)
- Riemer, N., Vogel, H., Vogel, B., and Fiedler, F.: Modeling aerosol on the mesoscale-y: Treatment of soot aerosol and its radiative effects, *J. Geophys. Res.*, 108(D4), 4601, doi:10.1029/2003JD003448, 108. [9933](#)

MATRIX

S. E. Bauer et al.

Title Page

Abstract

Introduction

Conclusions

References

Tables

Figures

◀

▶

◀

▶

Back

Close

Full Screen / Esc

Printer-friendly Version

Interactive Discussion



Schmidt, G. A., Ruedy, R., Hansen, J., Aleinov, I., Bell, N., Bauer, M., Bauer, S., Cairns, B., Cheng, Y., DelGenio, A., Faluvegi, G., Friend, A., Hall, T. M., Hu, Y., Kelley, M., Kiang, N., Koch, D., Lacis, A. A., Lerner, J., Lo, K. K., Miller, R. L., Nazarenko, L., Oinas, V., Perlwitz, J., Perlwitz, J., Rind, D., Romanou, A., Russell, G. L., Shindell, D. T., Stone, P. H., Sun, S., Tausnev, N., and Yao, M.-S.: Present day atmospheric simulations using GISS ModelE: Comparison to in-situ, satellite and reanalysis data, *J. Climate*, 19, 153–192, 2006. [9934](#), [9953](#)

Schwarz, J. P. and et al.: Single-particle measurements of midlatitude black carbon and light-scattering aerosols from the boundary layer to the lower stratosphere, *J. Geophys. Res.*, 111, D16207, doi:10.1029/2006JD007076, 2006. [9958](#), [9959](#), [9993](#)

Schwarz, J. P., Spackman, J. R., Fahey, D. W., Gao, R. S., Lohmann, U., Stier, P., Watts, L. A., Thomson, D. S., Lack, D. A., Pfister, L., Mahoney, M. J., Baumgardner, D., Wilson, J. C., and Reeves, J. M.: Coatings and their enhancement of black-carbon light absorption in the tropical atmosphere, *J. Geophys. Res.*, 113, D03203, doi:10.1029/2007JD009042, 2008. [9958](#), [9993](#)

Seinfeld, J. H. and Pandis, S. N.: *Atmospheric Chemistry and Physics. From Air Pollution to Climate Change*, John Wiley and Sons, Inc. New York, 1998. [9945](#)

Shindell, D. T., Faluvegi, G., and Bell, N.: Preindustrial-to-present-day radiative forcing by tropospheric ozone from improved simulations with the GISS chemistry-climate GCM, *Atmos. Chem. Phys.*, 3, 1675–1702, 2003, <http://www.atmos-chem-phys.net/3/1675/2003/>. [9953](#)

Singh, H., Brune, W., Crawford, J., and et al.: Overview of the summer 2004 intercontinental chemical transport experiment – North America (INTEX-A), *J. Geophys. Res.*, 111, D24S01, doi:10.1029/2006JD007905, 2006. [9961](#)

Stier, P., Feichter, J., Kinne, S., Kloster, S., Vignati, E., Wilson, J., Ganzeveld, L., Tegen, I., Werner, M., Balkanski, Y., Schulz, M., Boucher, O., Minikin, A., and Petzold, A.: The aerosol-climate model ECHAM5-HAM, *Atmos. Chem. Phys.*, 5, 1125–1156, 2005, <http://www.atmos-chem-phys.net/5/1125/2005/>. [9933](#)

Turco, R., Zhao, J., and Yu, F.: A new source of tropospheric aerosols: Ion-ion recombination, *Geophys. Res. Lett.*, 25, 635–638, 1998. [9942](#), [9943](#), [9951](#), [9955](#)

van der Werf, G. R., Randerson, J., Collatz, G., and Giglio, L.: Carbon emission from fires in tropical and subtropical ecosystems, *Global change Biology*, 9, 547–562, 2003. [9954](#)

Vehkamäki, H., Kulmala, M., Napari, I., Lehtinen, K., Timmreck, C., Noppel, M., and Laak-

MATRIX

S. E. Bauer et al.

[Title Page](#)[Abstract](#)[Introduction](#)[Conclusions](#)[References](#)[Tables](#)[Figures](#)[I◀](#)[▶I](#)[◀](#)[▶](#)[Back](#)[Close](#)[Full Screen / Esc](#)[Printer-friendly Version](#)[Interactive Discussion](#)

sonen, A.: An improved parameterization for sulfuric acid-water nucleation rates for tropo-
spheric and stratospheric conditions, *J. Geophys. Res.*, 107, 2002. [9942](#), [9943](#)

Whitby, E. R., Stratmann, F., and Wilck, M.: Merging and remapping modes in modal aerosol
dynamics models: a Dynamic Mode Manager, *J. of Aerosol Science*, 33 (4), 623–645, 2002.
[9950](#)

Wilson, J., Cuvelier, C., and Raes, F.: A modeling study of global mixed aerosol fields., *J.*
Geophys. Res., 106, 34,081–34,108, 2001. [9933](#), [9950](#)

Wright, D., McGraw, R., Benkovitz, C., and Schwartz, S.: Six-moment representation of multiple
aerosol populations in a sub-hemispheric chemical transformation model., *Geo. Res. Lett.*,
27, 967–970, 2000. [9933](#)

Wright, D., Kasibhatla, P., McGraw, R., and Schwartz, S.: Description and evaluation of a six-
moment aerosol microphysical module for use in atmospheric chemical transport models., *J.*
Geophys. Res., 106, 20 275–20 291., 2001. [9933](#)

Wright, D. L.: Numerical advection of moments of the particle size distribution in Eulerian
models, *J. of aerosol Sciences*, 38(3), 352–369, 2007. [9934](#)

Yu, S., Kasibhatla, P., Wright, D., Schwartz, S., McGraw, R., and Deng, A.: Moment-based
simulation of microphysical properties in the eastern United States: Model description, eval-
uation, and regional analysis, *J. Geophys. Res.*, 108, 4353, doi:10.1029/2002JD002890,
2003. [9933](#)

MATRIX

S. E. Bauer et al.

Table 1. (a) Modes, constituents, and transported species for aerosol mechanism 1.

mode description	symbol	constituents other than NH_4^+ , NO_3^- , and H_2O	transported species	$D_{g,N}$	$\sigma_{g,N}$	$D_{g,E}$	$\sigma_{g,E}$
sulfate Aitken mode	AKK	SO_4^{-2}	$N_{\text{AKK}}, M_{\text{AKK},\text{SO}_4}$	0.026	1.6	0.013	1.6
sulfate accum. Mode	ACC	SO_4^{-2}	$N_{\text{ACC}}, M_{\text{ACC},\text{SO}_4}$	0.11	1.8	0.068	1.8
dust accum. mode ($\leq 5\%$ inorg.)	DD1	mineral dust, SO_4^{-2}	$N_{\text{DD1}}, M_{\text{DD1},\text{dust}}, M_{\text{DD1},\text{SO}_4}$	0.58	1.8	0.58	1.8
dust accum. mode ($> 5\%$ inorg.)	DS1	mineral dust, SO_4^{-2}	$N_{\text{DS1}}, M_{\text{DS1},\text{dust}}, M_{\text{DS1},\text{SO}_4}$	0.58	1.8	–	–
dust coarse mode ($\leq 5\%$ inorg.)	DD2	mineral dust, SO_4^{-2}	$N_{\text{DD2}}, M_{\text{DD2},\text{dust}}, M_{\text{DD2},\text{SO}_4}$	5.4	1.8	5.4	1.8
dust coarse mode ($> 5\%$ inorg.)	DS2	mineral dust, SO_4^{-2}	$N_{\text{DS2}}, M_{\text{DS2},\text{dust}}, M_{\text{DS2},\text{SO}_4}$	5.4	1.8	–	–
sea salt accum.. mode	SSA	sea salt, SO_4^{-2}	$M_{\text{SSA},\text{seasalt}}$	0.37	1.8	0.37	1.8
sea salt coarse mode	SSC	sea salt, SO_4^{-2}	$M_{\text{SSC},\text{seasalt}}, M_{\text{SSC},\text{SO}_4} + M_{\text{SSA},\text{SO}_4}$	3.93	2.0	3.93	2.0
OC	OCC	OC, SO_4^{-2}	$N_{\text{OCC}}, M_{\text{OCC},\text{OC}}, M_{\text{OCC},\text{SO}_4}$	0.053	1.8	0.030	1.8
BC ($\leq 5\%$ inorg.)	BC1	BC, SO_4^{-2}	$N_{\text{BC1}}, M_{\text{BC1},\text{BC}}, M_{\text{BC1},\text{SO}_4}$	0.053	1.8	0.030	1.8
BC (5–20% inorg.)	BC2	BC, SO_4^{-2}	$N_{\text{BC2}}, M_{\text{BC2},\text{BC}}, M_{\text{BC2},\text{SO}_4}$	0.054	1.8	–	–
BC ($> 20\%$ inorg.)	BC3	BC, SO_4^{-2}	$N_{\text{BC3}}, M_{\text{BC3},\text{BC}}, M_{\text{BC3},\text{SO}_4}$	0.057	1.8	–	–
BC–mineral dust	DBC	BC, mineral dust, SO_4^{-2}	$N_{\text{DBC}}, M_{\text{DBC},\text{dust}}, M_{\text{DBC},\text{BC}}, M_{\text{DBC},\text{SO}_4}$	0.33	1.8	–	–
BC–OC	BOC	BC, OC, SO_4^{-2}	$N_{\text{BOC}}, M_{\text{BOC},\text{BC}}, M_{\text{BOC},\text{OC}}, M_{\text{BOC},\text{SO}_4}$	0.067	1.8	0.037	1.8
BC–sulfate	BSC	BC, SO_4^{-2}	$N_{\text{BSC}}, M_{\text{BSC},\text{BC}}, M_{\text{BSC},\text{SO}_4}$	0.070	1.8	–	–
Mixed	MXX	BC, OC, mineral dust, sea salt, SO_4^{-2}	$N_{\text{MXX}}, M_{\text{MXX},\text{BC}}, M_{\text{MXX},\text{OC}}, M_{\text{MXX},\text{dust}}, M_{\text{MXX},\text{seasalt}}, M_{\text{MXX},\text{SO}_4}$	0.30	2.0	–	–

Title Page

Abstract

Introduction

Conclusions

References

Tables

Figures

◀

▶

◀

▶

Back

Close

Full Screen / Esc

Printer-friendly Version

Interactive Discussion



MATRIX

S. E. Bauer et al.

Table 1. (b) Coagulation interactions for aerosol mechanism 1. Donor modes are in bold font, receptor modes in normal font.

	donor mode															
donor mode	AKK	ACC	DD1	DS1	DD2	DS2	SSA	SSC	OCC	BC1	BC2	BC3	DBC	BOC	BCS	MXX
AKK	AKK	ACC	DD1	DS1	DD2	DS2	SSA	SSC	OCC	BCS	BCS	BCS	DBC	BOC	BCS	MXX
ACC	ACC	ACC	DD1	DS1	DD2	DS2	SSA	SSC	OCC	BCS	BCS	BCS	DBC	BOC	BCS	MXX
DD1	DD1	DD1	DD1	DD1	DD2	DD2	MXX	MXX	MXX	DBC	DBC	DBC	DBC	MXX	DBC	MXX
DS1	DS1	DS1	DD1	DS1	DD2	DS2	MXX	MXX	MXX	DBC	DBC	DBC	DBC	MXX	DBC	MXX
DD2	DD2	DD2	DD2	DD2	DD2	DD2	MXX	MXX	MXX	DBC	DBC	DBC	DBC	MXX	DBC	MXX
DS2	DS2	DS2	DD2	DS2	DD2	DS2	MXX	MXX	MXX	DBC	DBC	DBC	DBC	MXX	DBC	MXX
SSA	SSA	SSA	MXX	MXX	MXX	MXX	SSA	SSC	MXX							
SSC	SSC	SSC	MXX	MXX	MXX	MXX	SSC	SSC	MXX							
OCC	OCC	OCC	MXX	MXX	MXX	MXX	MXX	MXX	OCC	BOC	BOC	BOC	MXX	BOC	BOC	MXX
BC1	BCS	BCS	DBC	DBC	DBC	DBC	MXX	MXX	BOC	BC1	BC1	BC1	DBC	BOC	BCS	MXX
BC2	BCS	BCS	DBC	DBC	DBC	DBC	MXX	MXX	BOC	BC1	BC2	BC2	DBC	BOC	BCS	MXX
BC3	BCS	BCS	DBC	DBC	DBC	DBC	MXX	MXX	BOC	BC1	BC2	BC3	DBC	BOC	BCS	MXX
DBC	DBC	DBC	DBC	DBC	DBC	DBC	MXX	MXX	MXX	DBC	DBC	DBC	DBC	MXX	DBC	MXX
BOC	BOC	BOC	MXX	MXX	MXX	MXX	MXX	MXX	BOC	BOC	BOC	BOC	MXX	BOC	BOC	MXX
BCS	BCS	BCS	DBC	DBC	DBC	DBC	MXX	MXX	BOC	BCS	BCS	BCS	DBC	BOC	BCS	MXX
MXX	MXX	MXX	MXX	MXX	MXX	MXX	MXX	MXX	MXX	MXX	MXX	MXX	MXX	MXX	MXX	MXX

Title Page

Abstract

Introduction

Conclusions

References

Tables

Figures

I◀

▶I

◀

▶

Back

Close

Full Screen / Esc

Printer-friendly Version

Interactive Discussion



Table 2. Table of aerosol mechanisms.

mechanism number	number of modes	number of transported species	modes represented
1	16	51	AKK, ACC, DD1, DS1, DD2, DS2, SSA, SSC, OCC, BC1, BC2, BC3, BCS, DBC, BOC, MXX
2	16	51	AKK, ACC, DD1, DS1, DD2, DS2, SSA, SSC, OCC, BC1, BC2, OCS, BCS, DBC, BOC, MXX
3	13	41	AKK, ACC, DD1, DS1, DD2, DS2, SSA, SSC, OCC, BC1, BC2, BOC, MXX
4	10	34	ACC, DD1, DS1, DD2, DS2, SSS, OCC, BC1, BC2, MXX
5	14	45	AKK, ACC, DD1, DS1, SSA, SSC, OCC, BC1, BC2, BC3, BCS, DBC, BOC, MXX
6	14	45	AKK, ACC, DD1, DS1, SSA, SSC, OCC, BC1, BC2, OCS, BCS, DBC, BOC, MXX
7	11	35	AKK, ACC, DD1, DS1, SSA, SSC, OCC, BC1, BC2, BOC, MXX
8	8	28	ACC, DD1, DS1, SSS, OCC, BC1, BC2, MXX

MATRIX

S. E. Bauer et al.

Title Page

Abstract

Introduction

Conclusions

References

Tables

Figures



Back

Close

Full Screen / Esc

Printer-friendly Version

Interactive Discussion



Table 3. Annual mean budget per mode and microphysical process.

Specie	Emission [Gg/a]	Coag. Prod.	Loss	Conden. norm.	in cloud	Mode – Transfer Loss	Microphy. Σ	Wet – removal	Dry – removal	Load [Gg]	Lifetime [d]
AKK SU (npf)	4970.26 1224.61	–	–1854.18	934.22	8.49	–261.12	52.02	98.38	12.80	3.18	10.3
ACC SU	4920.56	473.36	–6638.14	2497.05	5954.48	359.44	2646.00	7087.00	999.30	80.42	3.5
DD1 SU	–	41.99	–211.84	149.25	77.89	–51.46	5.84	2.78	5.07	0.57	26.4
DS1 SU	–	3.77	–132.27	16.19	110.72	54.89	53.31	59.76	7.79	0.51	2.7
DD2 SU	–	0.07	–0.28	0.20	0.02	>–0.01	<0.01	<0.01	<0.01	<0.01	6.4
SSA SU	–	95.31	–227.22	133.07	529.47	–	264.50	223.40	41.83	2.34	3.1
OCC SU	–	4633.06	–8520.05	2459.31	13881.60	–	12450.00	12490.00	2366.00	233.80	5.6
BC1 SU	–	0.05	–3.14	4.28	<0.01	–1.02	0.18	0.12	0.10	0.01	6.1
BC2 SU	–	0.03	–1.35	1.24	<0.01	0.25	0.17	0.19	0.02	<0.01	8.0
BC3 SU	–	–	–5.44	1.03	21.72	0.80	18.10	16.64	1.74	0.04	8.8
DBC SU	–	42.70	–78.84	17.71	23.69	–	5.26	3.07	2.93	0.23	1.4
BOC SU	–	14492.30	–6436.39	6372.05	46947.60	–	61380.00	72800.00	16190.00	1535.00	6.2
BCS SU	–	947.99	–931.88	114.58	287.21	–	417.90	427.70	84.59	4.32	3.0
MXS SU	–	7702.44	–	2338.14	2669.56	–	12710.00	12390.00	4488.00	258.50	5.5
Σ SU (npf)	4970.26 1224.61							105599.04	24200.17	2118.87	5.84
BC1BC	4620.00	11.53	–3487.52	–	–	–606.99	–4083.00	364.50	331.30	2.04	1.0
BC2 BC	–	1.92	–252.86	–	–	328.55	77.62	82.30	12.53	34.43	1.3
BC3 BC	–	–	–181.20	–	–	285.26	104.10	104.10	11.30	28.88	0.9
DBC BC	–	5.29	–5.19	–	–	–	0.10	0.03	0.08	0.01	23.8
BOC BC	3689.72	3215.92	–152.21	–	–	–	3064.00	7983.00	2168.00	146.80	5.2
BCS BC	–	2786.81	–2138.31	–	–	–	648.50	562.60	228.00	12.12	5.5
MXS BC	–	188.97	–	–	–	–	189.00	208.40	57.66	4.50	6.1
Σ BC	8309.72							9304.93	2808.84	228.78	6.8
OCC OC	28466.10	–	–17161.80	–	–	–	–17160.00	11910.00	4847.00	166.90	3.5
BOC OC	30213.50	16553.10	–983.41	–	–	–	15770.00	55470.00	15350.00	1094.00	5.5
MXS OC	–	1592.18	–	–	–	–	1592.00	1749.00	512.30	37.55	5.9
Σ OC	58679.60							69129.00	20709.30	1298.45	5.2
DD1 DU	676854.00	33.57	–642927.00	–	–	–13021.80	–655900.00	1320.00	20300.00	634.40	10.5
DS1 DU	–	–	–7760.30	–	–	12943.10	5183.00	5236.00	721.52	37.10	2.2
DD2 DU	962184.00	8.59	–924474.00	–	–	–31.54	–924500.00	56.91	37650.00	28.66	0.2
DS2 DU	–	0.01	–15.19	–	–	30.64	15.45	13.21	2.53	0.04	1.0
DBC DU	–	184360.00	–176992.00	–	–	–	7368.00	410.52	7107.00	154.10	7.3
MXS DU	–	1567850.00	–	–	–	–	1568000.00	1459000.00	699000.00	48930.00	8.1
Σ DU	1639038.00							1466036.64	764781.05	49784.30	8.0
SSA SS	421389.00	–	–286874.00	–	–	–	–286900.00	107400.00	27080.00	674.40	1.8
SSC SS	1553750.00	2.39	–1226670.00	–	–	–	–1227000.00	64760.00	320600.00	25.20	0.2
MXS SS	–	1513550.00	–	–	–	–	1514000.00	830200.00	710400.00	5170.00	1.2
Σ SS	1975139.00							944076.00	1058080.00	5869.60	1.1



MATRIX

S. E. Bauer et al.

Title Page

Abstract

Introduction

Conclusions

References

Tables

Figures

◀

▶

◀

▶

Back

Close

Full Screen / Esc

Printer-friendly Version

Interactive Discussion

**Table 4.** Annual mean budget of transported bulk species.

Specie	Emission [Gg/a]	Wet – removal	Dry – removal	Load [Gg]	Lifetime [d]
SO ₂	169280.	96170	39760.	1284.	3.4
DMS	423918.				
NH ₃	641415.	2653.	904.	13.40	1.4
NH ₄	–	33140.	7395.	466.30	4.2
NO ₃	–	7690.	4787.	160.11	4.6
H ₂ O	–	3316.	394.	10.83	1.0

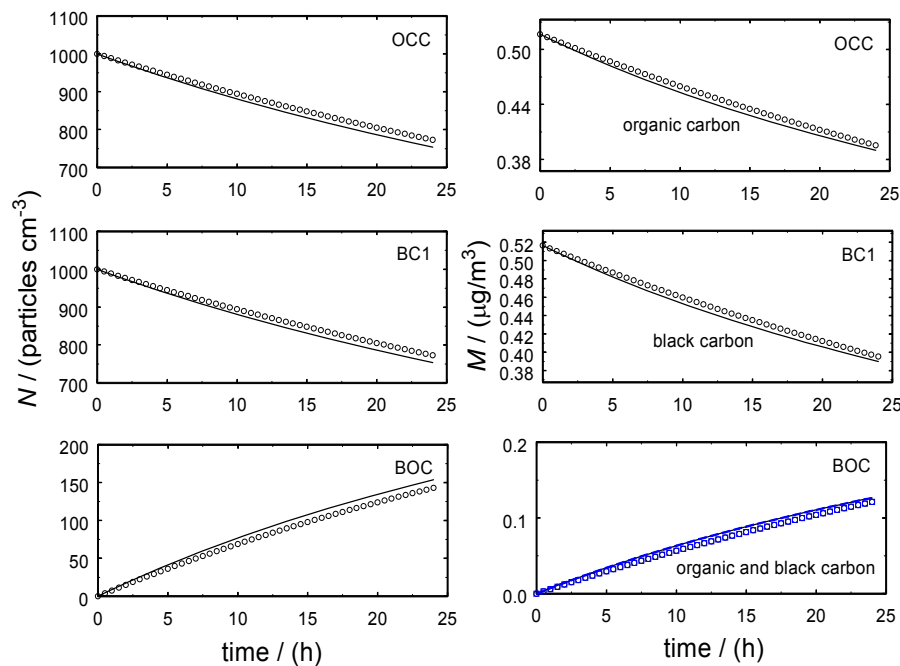


Fig. 1. Number and mass concentrations as a function of time for the coagulation of modes OCC and BC1 to form mode BOC. Solid lines are accurate results from MATRIX applied as a discrete model, open symbols are results from the standard MATRIX model.

[Title Page](#)[Abstract](#)[Introduction](#)[Conclusions](#)[References](#)[Tables](#)[Figures](#)[◀](#)[▶](#)[◀](#)[▶](#)[Back](#)[Close](#)[Full Screen / Esc](#)[Printer-friendly Version](#)[Interactive Discussion](#)

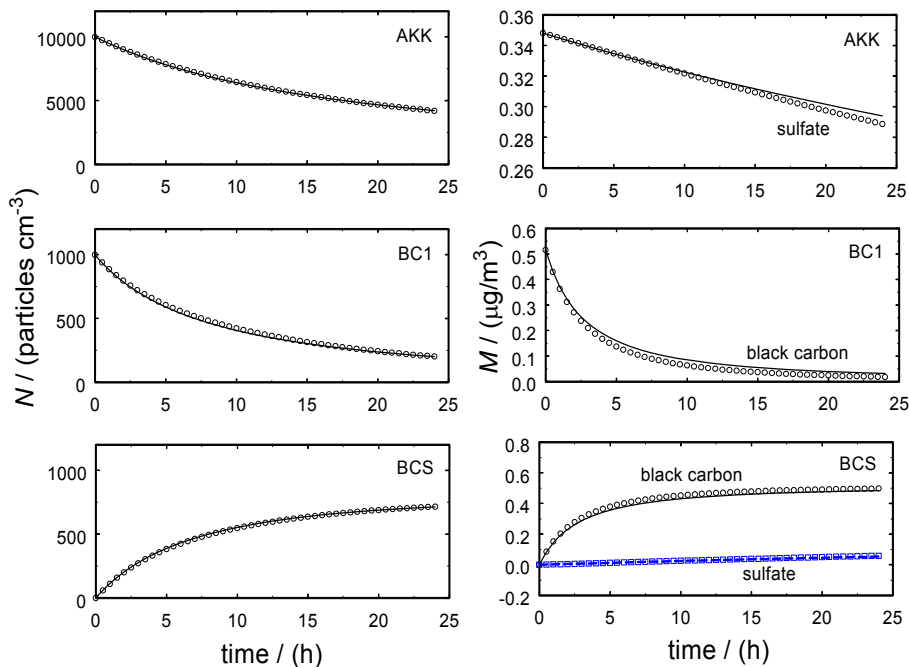


Fig. 2. Number and mass concentrations as a function of time for the coagulation of modes AKK and BC1 to form mode BCS. Line styles the same as in Fig. 1.

[Title Page](#)[Abstract](#)[Introduction](#)[Conclusions](#)[References](#)[Tables](#)[Figures](#)[◀](#)[▶](#)[◀](#)[▶](#)[Back](#)[Close](#)[Full Screen / Esc](#)[Printer-friendly Version](#)[Interactive Discussion](#)

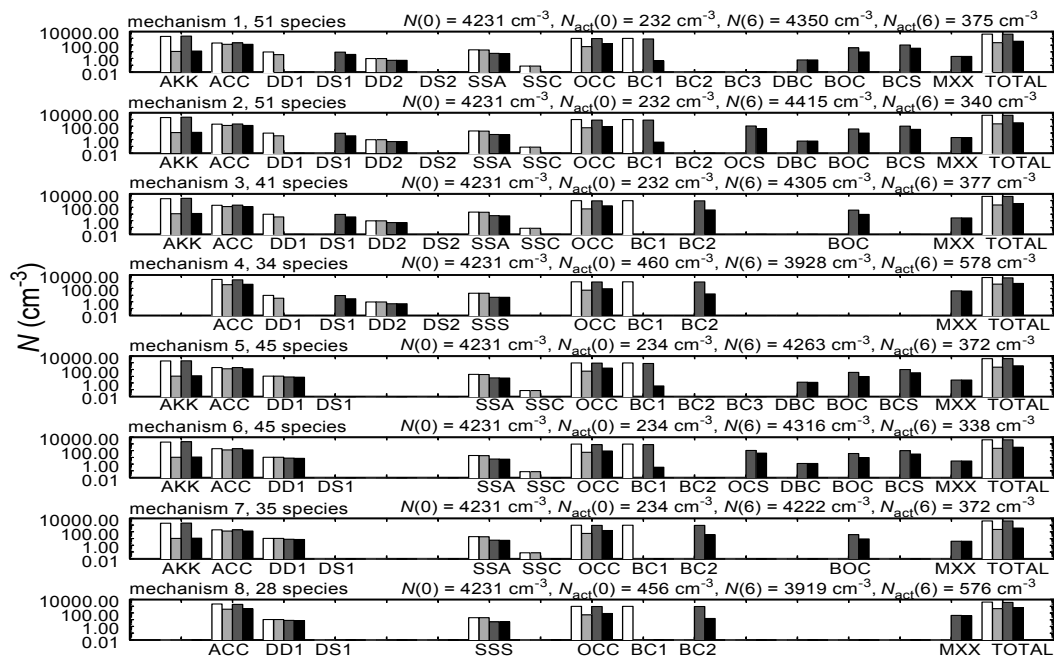


Fig. 3. Illustration of cloud activation for each of the eight aerosol mechanisms. White bars are initial total number concentrations, light-gray bars are initial activating number concentrations, dark gray bars are total number concentrations after 6 h evolution, black bars are activating number concentrations after 6 h evolution.

[Title Page](#)
[Abstract](#)
[Introduction](#)
[Conclusions](#)
[References](#)
[Tables](#)
[Figures](#)
[Back](#)
[Close](#)
[Full Screen / Esc](#)
[Printer-friendly Version](#)
[Interactive Discussion](#)

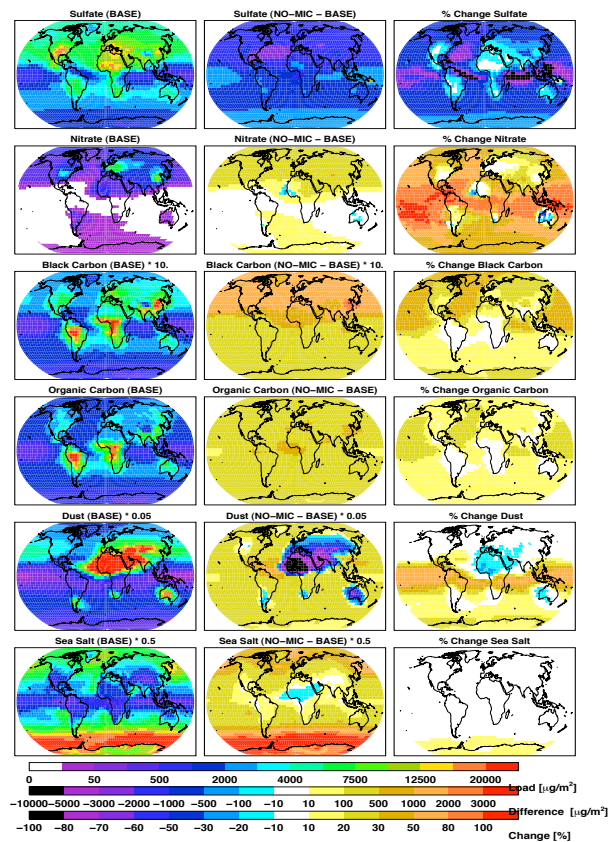



Fig. 4. Column mean load per specie (left column) and difference between NO-MIC and BASE (middle column) in units of $[\mu\text{g}/\text{m}^3]$. The right column presents the percentage change of NO-MIC in respect to the BASE simulation $[(\text{NO-MIC}-\text{BASE})/\text{NO-MIC}]$ in [%]. Note that the load and difference plots of black carbon, dust and sea salt are multiplied by a factor, given in the maps title, to match the color bar scheme.

[Title Page](#)
[Abstract](#)
[Introduction](#)
[Conclusions](#)
[References](#)
[Tables](#)
[Figures](#)
[◀](#)
[▶](#)
[◀](#)
[▶](#)
[Back](#)
[Close](#)
[Full Screen / Esc](#)
[Printer-friendly Version](#)
[Interactive Discussion](#)

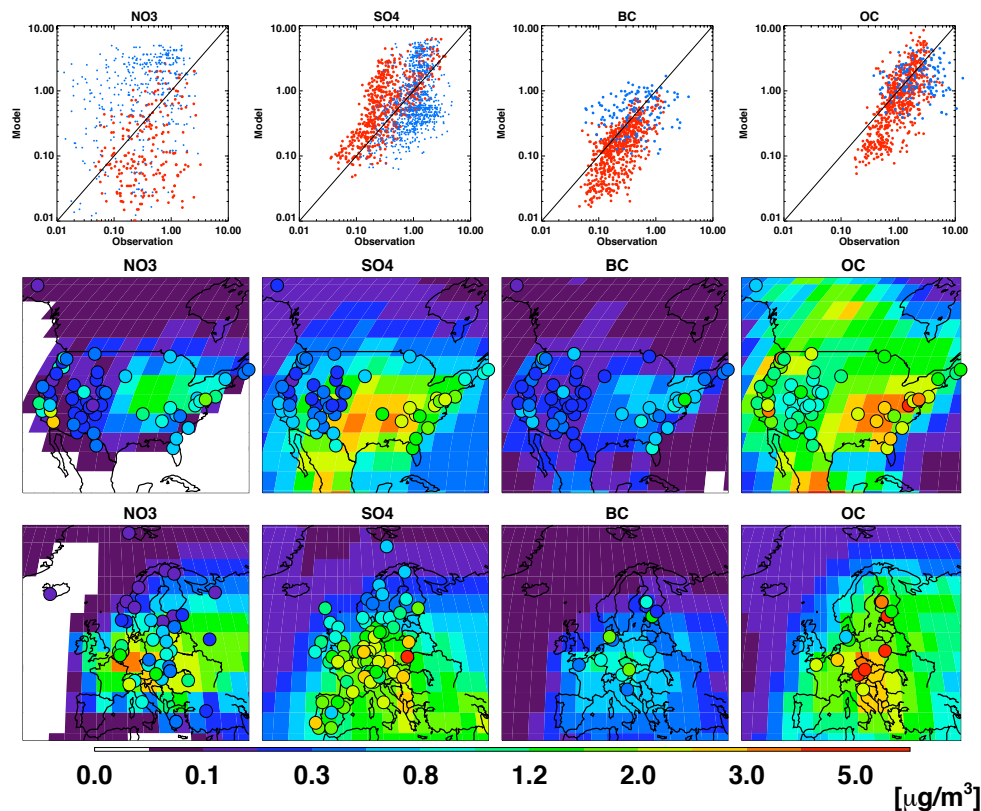



Fig. 5. Scatter plots (first line) and maps of surface mass concentrations of nitrate, sulfate, black and organic carbon as compared to the IMPROVE data set over North America and the EMEP observation data over Europe. The blue points in the scatter plots show comparison of the EMEP stations, and the red points to the IMPROVE network stations. The measured surface observations are presented as filled circles. Units are $[\mu\text{g}/\text{m}^3]$.

[Title Page](#)[Abstract](#)[Introduction](#)[Conclusions](#)[References](#)[Tables](#)[Figures](#)[◀](#)[▶](#)[◀](#)[▶](#)[Back](#)[Close](#)[Full Screen / Esc](#)[Printer-friendly Version](#)[Interactive Discussion](#)

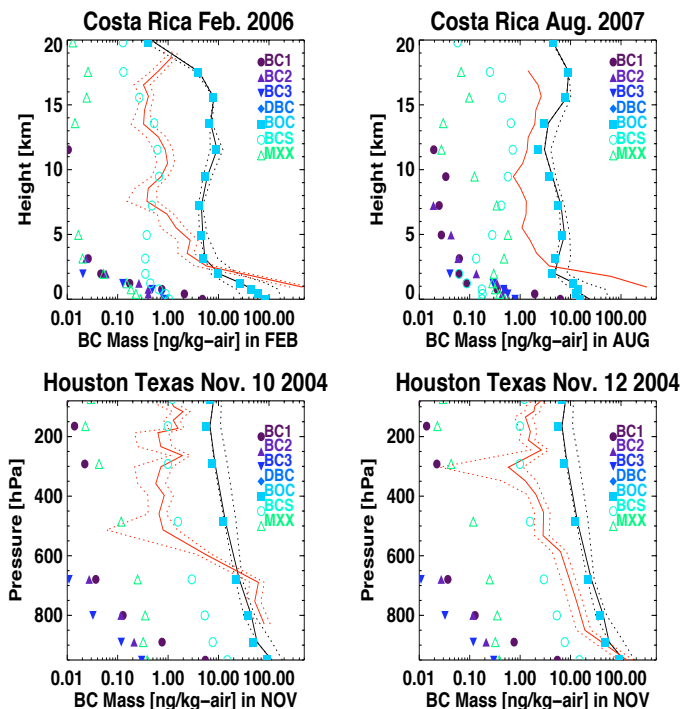


Fig. 6. Vertical black carbon mass concentrations as observed (red line) over Costa Rica (upper panel) in February 2006 and August 2007 (mean over three flights), and two single flights over Houston, Texas (lower panel) in November 2004 (Schwarz et al., 2008; Schwarz and et al., 2006). The total simulated BC mass (black line) and its contribution for the single modes are shown (colored symbols). Units are [ng/kg-air]. Height in [Km] (upper panel) and on pressure levels [hPa] (lower panel).

[Title Page](#)
[Abstract](#)
[Introduction](#)
[Conclusions](#)
[References](#)
[Tables](#)
[Figures](#)
[Back](#)
[Close](#)
[Full Screen / Esc](#)
[Printer-friendly Version](#)
[Interactive Discussion](#)


MATRIX

S. E. Bauer et al.

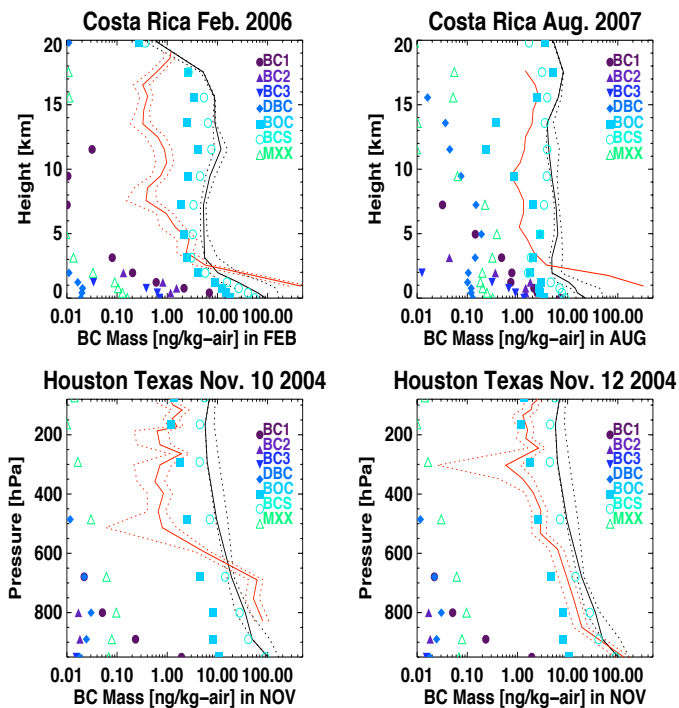


Fig. 7. Like Fig. 6, but presenting model results of Exp. 2.

[Title Page](#)[Abstract](#)[Introduction](#)[Conclusions](#)[References](#)[Tables](#)[Figures](#)[◀](#)[▶](#)[◀](#)[▶](#)[Back](#)[Close](#)[Full Screen / Esc](#)[Printer-friendly Version](#)[Interactive Discussion](#)

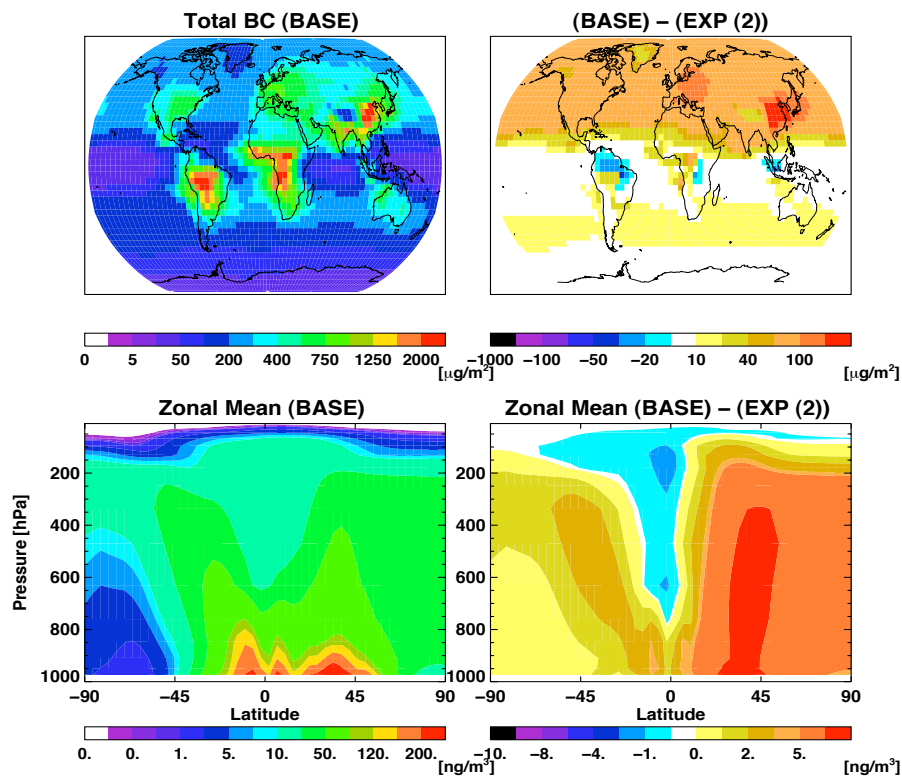


Fig. 8. Total column and zonal mean concentrations of BC for the BASE experiment and differences between BASE and Exp. 2.

[Title Page](#)[Abstract](#)[Introduction](#)[Conclusions](#)[References](#)[Tables](#)[Figures](#)[◀](#)[▶](#)[◀](#)[▶](#)[Back](#)[Close](#)[Full Screen / Esc](#)[Printer-friendly Version](#)[Interactive Discussion](#)

MATRIX

S. E. Bauer et al.

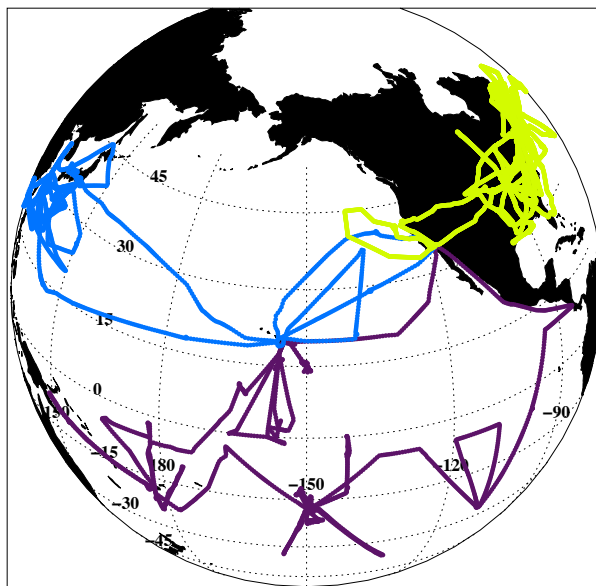


Fig. 9. Flight tracks of the INTEX (green), Trace P (blue) and PEM Tropics (purple) campaign.

[Title Page](#)[Abstract](#)[Introduction](#)[Conclusions](#)[References](#)[Tables](#)[Figures](#)[◀](#)[▶](#)[◀](#)[▶](#)[Back](#)[Close](#)[Full Screen / Esc](#)[Printer-friendly Version](#)[Interactive Discussion](#)

MATRIX

S. E. Bauer et al.

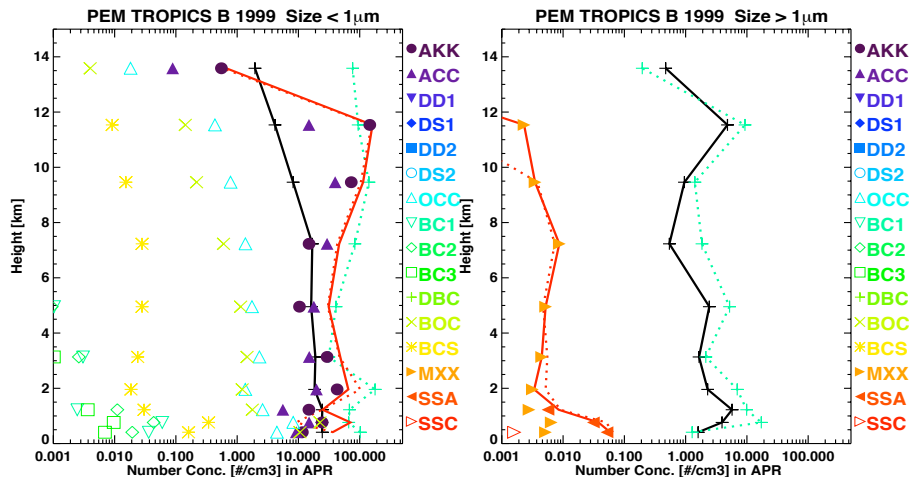


Fig. 10. Vertical profiles of number concentrations as measured by the FSSP (green dotted line) and PCASP (black solid line) aerosol probe on board of the DC-8 air plane are compared to the model results (red line). Number concentrations for particles smaller (left) and larger (right) than $1\ \mu\text{m}$ diameter are shown. The symbols indicate the contribution to the total number concentrations from the single modes as marked in the graph. Units are $[\text{particles}/\text{cm}^3]$.

[Title Page](#)
[Abstract](#)
[Introduction](#)
[Conclusions](#)
[References](#)
[Tables](#)
[Figures](#)
[◀](#)
[▶](#)
[◀](#)
[▶](#)
[Back](#)
[Close](#)
[Full Screen / Esc](#)
[Printer-friendly Version](#)
[Interactive Discussion](#)

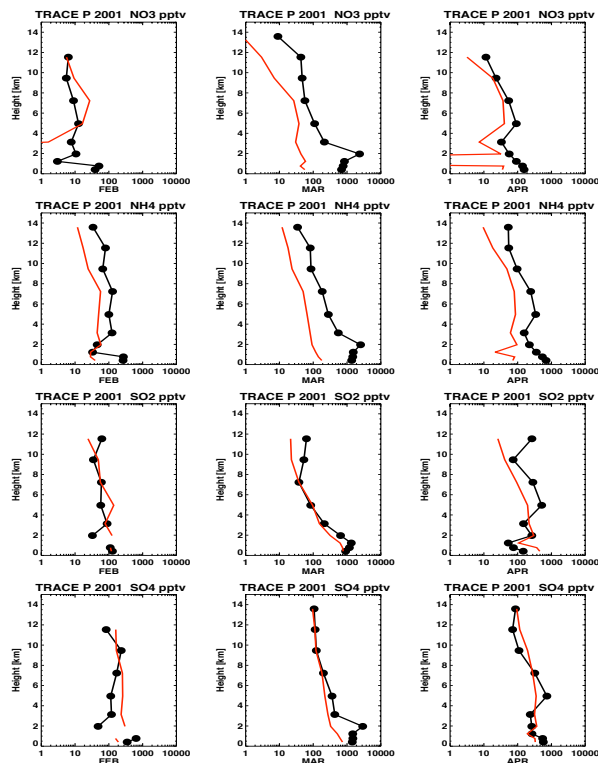



Fig. 11. Vertical profiles of mass concentrations for the month of February (left column), March (middle column) and April (right column) during the TRACE – P campaign in 2001. Measurements by the DC-8 air craft are printed in black, and model results are shown in red. The black dots indicate the model layers onto which the measured data points were interpolated. Following species are presented per row: nitrate, ammonia, sulfur dioxide and sulfate. Units are [ppt_v].

[Title Page](#)[Abstract](#)[Introduction](#)[Conclusions](#)[References](#)[Tables](#)[Figures](#)[◀](#)[▶](#)[◀](#)[▶](#)[Back](#)[Close](#)[Full Screen / Esc](#)[Printer-friendly Version](#)[Interactive Discussion](#)

MATRIX

S. E. Bauer et al.

Title Page

Abstract

Introduction

Conclusions

References

Tables

Figures

◀

▶

◀

▶

Back

Close

Full Screen / Esc

Printer-friendly Version

Interactive Discussion

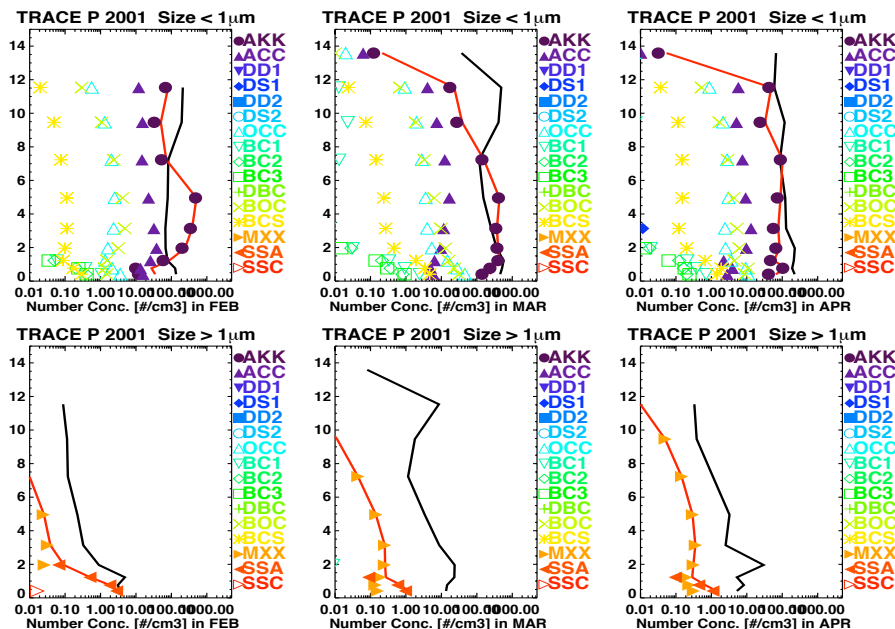


Fig. 12. Vertical number concentrations for the month of February (left column), March (middle column) and April (right column) during the TRACE – P campaign in 2001. Observations are shown in black, model data are presented as described in Fig. 10. Units are $[\text{particles}/\text{cm}^3]$.

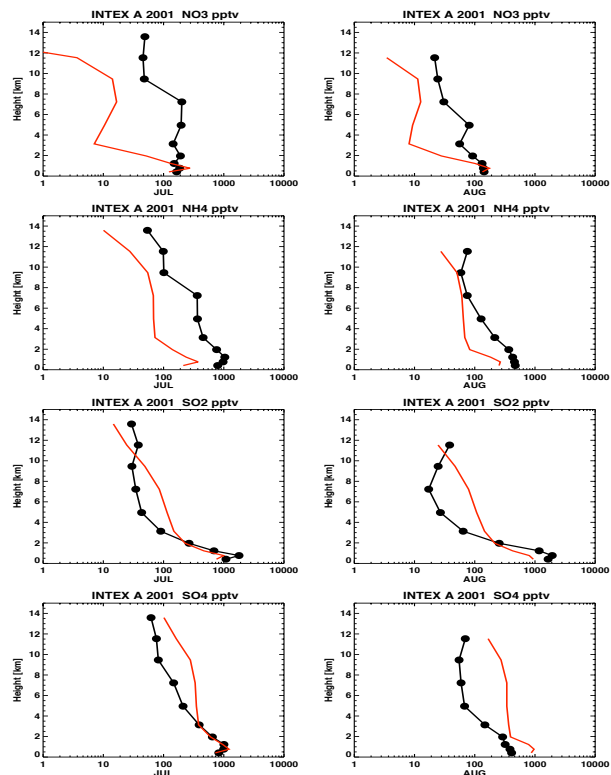


Fig. 13. Vertical profiles of mass concentrations for the month of July (left column), and August (right column) during the INTEX-A campaign in 2001. Measurements by the DC-8 air craft are printed in black, and model results are shown in red. The black dot's indicate the model layers onto which the measured data points where interpolated. Following species are presented per row: nitrate, ammonia, sulfur dioxide and sulfate. Units are [ppt_v].

[Title Page](#)[Abstract](#)[Introduction](#)[Conclusions](#)[References](#)[Tables](#)[Figures](#)[◀](#)[▶](#)[◀](#)[▶](#)[Back](#)[Close](#)[Full Screen / Esc](#)[Printer-friendly Version](#)[Interactive Discussion](#)

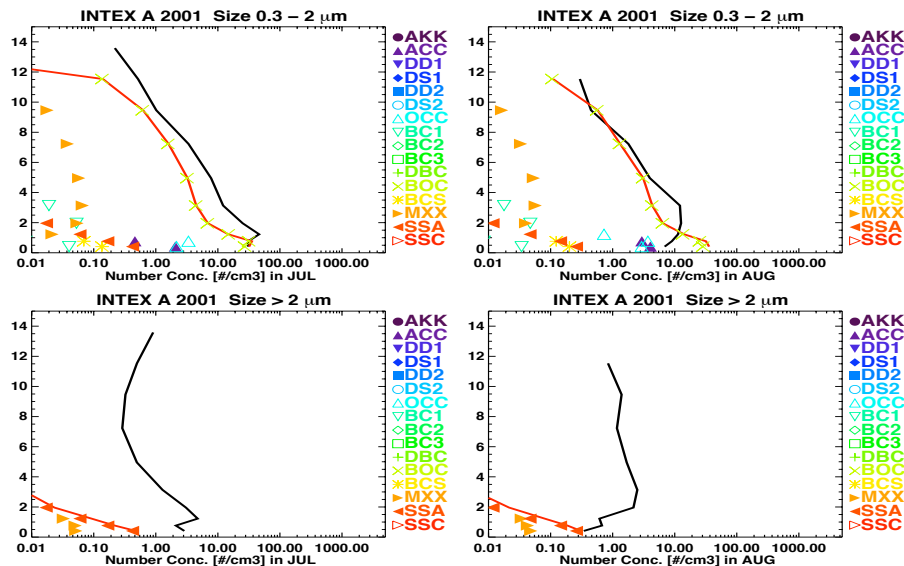


Fig. 14. Vertical number concentrations as observed during the INTEX-A campaign in 2001, for aerosol particles of the size of 0.3 to 2. and larger than 2 μm . Color coding as in Fig. 10. Units are [particles/cm³].

[Title Page](#)
[Abstract](#)
[Introduction](#)
[Conclusions](#)
[References](#)
[Tables](#)
[Figures](#)
[◀](#)
[▶](#)
[◀](#)
[▶](#)
[Back](#)
[Close](#)
[Full Screen / Esc](#)
[Printer-friendly Version](#)
[Interactive Discussion](#)

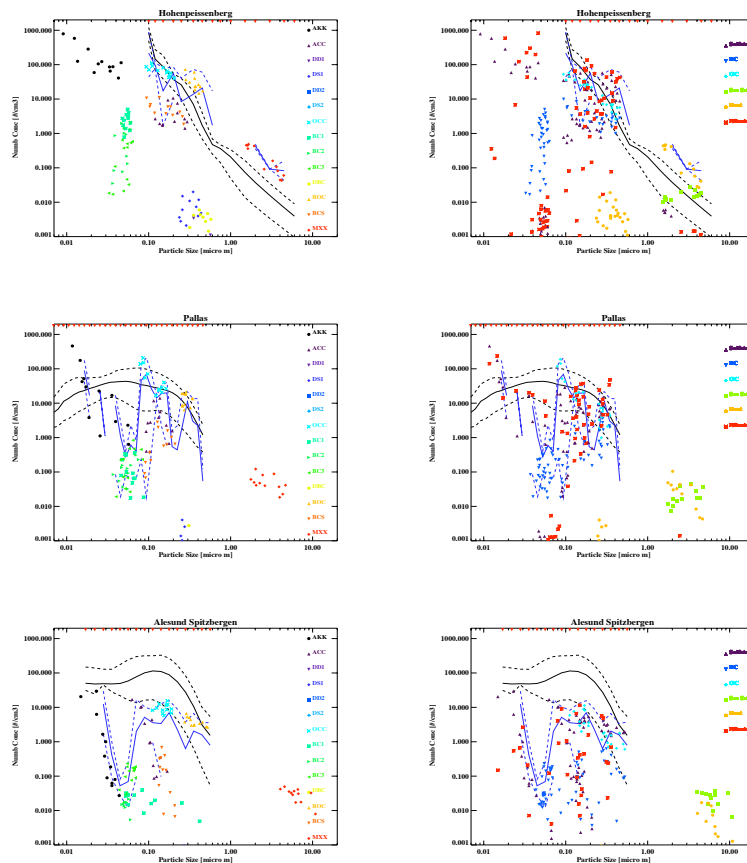



Fig. 15. Aerosol size distribution at three surface stations: Hohenpeißenberg (upper panels), Pallas (middle panels) and Ålesund (lower panels). The observed size distributions are shown in black, and simulated size distributions in blue. The solid line show the annual mean values and the dotted lines the seasonal maxima and minima. The red triangles at the top of the graph indicated the size bins of the observational data, into which the modelled data have been interpolated. The colored symbols in the graphs in the right column indicate the contribution to the particles number concentration by mode, and in the left column by specie. Units are [μm] and [$\text{particles}/\text{cm}^3$].

[Title Page](#)
[Abstract](#)
[Introduction](#)
[Conclusions](#)
[References](#)
[Tables](#)
[Figures](#)
[Back](#)
[Close](#)
[Full Screen / Esc](#)
[Printer-friendly Version](#)
[Interactive Discussion](#)


MATRIX

S. E. Bauer et al.

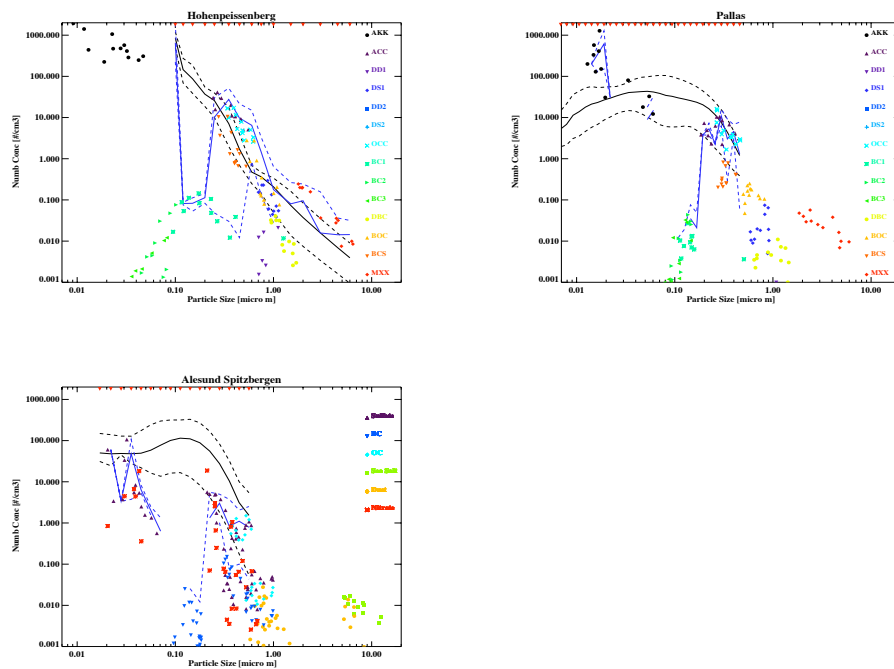


Fig. 16. Like the left column of Fig. 15, but for Exp. 2.

[Title Page](#)[Abstract](#)[Introduction](#)[Conclusions](#)[References](#)[Tables](#)[Figures](#)[Back](#)[Close](#)[Full Screen / Esc](#)[Printer-friendly Version](#)[Interactive Discussion](#)